THE INVESTIGATION OF THE WATER SPLITTING ACTIVITIES OF COPRECIPITATED DOPED NANOTITANIA POWDERS

A Thesis Submitted to
the Graduate School of Engineering and Sciences of
İzmir Institute of Technology
in Partial Fulfillment of the Requirements for the Degree of

MASTER OF SCIENCE

in Chemical Engineering

by
Gözde GÖZEL

July 2018
İZMİR

We approve the thesis of **Gözde GÖZEL**

Examining Committee Members:

_____
Prof. Dr. Muhsin ÇİFTÇİOĞLU
Department of Chemical Engineering, İzmir Institute of Technology

_____
Assist. Prof. Dr. Ayben TOP
Department of Chemical Engineering, İzmir Institute of Technology

_____
Assist. Prof. Dr. Canan URAZ
Department of Chemical Engineering, Ege University

6 July 2018

_____
Prof. Dr. Muhsin ÇİFTÇİOĞLU
Supervisor, Department of Chemical Engineering
İzmir Institute of Technology

_____
Prof. Dr. Erol ŞEKER
Head of the Department of Chemical Engineering

_____
Prof. Dr. Aysun SOFUOĞLU
Dean of the Graduate School of Engineering and Sciences

ACKNOWLEDGEMENTS

First of all, I would like to express my gratefullness to my advisor, Prof. Dr. Muhsin ÇİFTÇİOĞLU for his guidance, motivation, support and encouragement during my M.Sc. Thesis.

I would like to thank to Hüsnü Arda YURTSEVER and Burcu ALP for their assistance during this study.

I am also grateful to my laboratory colleagues, Pınar ÇETİN, Gupse Ayşe TURAN and Kaan YALTRIK for their support, friendships and assistance to my work.

I would like to thank İzmir Institute of Technology Center For Materials Research (IZTECH MAM) for providing technical support and help.

Finally, I express my sincere thanks to my family İbrahim GÖZEL, Sevgi GÖZEL and Özge GÖZEL for their love, support, encouragament and patience throughout my education.

ABSTRACT

THE INVESTIGATION OF THE WATER SPLITTING ACTIVITIES OF COPRECIPITATED DOPED NANOTITANIA POWDERS

The increase in the extent of greenhouse gases in earth's atmosphere lies behind the global warming and climate change. The extensive use of unsustainable fossil fuels have intensified the greenhouse effect, causing global warming. Hydrogen is considered as an ideal fuel for the future. Hydrogen fuel can be produced from renewable energy sources and its life cycle is clean. Artificial photosynthesis has been considered as a promising prospect for the synthesis of renewable and sustainable fuels. Photocatalysis is expected to make a great contribution to environmental problems and renewable energy generation in the very near future. Titania based photocatalytic materials are one of the widely used materials in artificial photosynthesis research due to their unique chemical and optical properties. Photocatalytic water-splitting by using TiO_2 based photocatalysts for hydrogen production offers a promising alternative for clean, low-cost and environmentally friendly production of hydrogen.

ZrO_2 doped TiO_2 photocatalyst powders were prepared by coprecipitation and characterized in this work. The photocatalytic water splitting activities of these ZrO_2 doped TiO_2 photocatalyst powders in hydrogen production was investigated under UV-Vis light. The phase structures of the powders were significantly affected by the level of dopants and the primary particle sizes increased from about 130 nm to about 500 nm during heat treatments in the 550-700°C range. Maximum hydrogen yield of about 5000 μmol/hr gcat. was obtained with the 550°C heat treated powder doped at 0.1-0.1 mol% ZrO_2-Nd_2O_3 level. ZrO_2 doping above 10 mol% decreased the hydrogen yields of the catalysts to lower than 1000 μmol/hr gcat.

ÖZET

BİRLİKTE ÇÖKTÜRÜLMÜŞ KATKILI NANOTİTANYA TOZLARININ SU PARÇALAMA AKTİVİTELERİNİN İNCELENMESİ

Küresel ısınma ve iklim değişikliğinin altında yatan ana neden atmosferdeki sera gazlarının artışıdır. Sürdürülemez fosil yakıtların geniş çaplı kullanımı sera gazı efektini arttırmakta, küresel ısınmaya sebep olmaktadır. Hidrojen gelecek için ideal yakıt olarak düşünülmektedir. Hidrojen yakıtı temiz ve yenilenebilir enerji kaynaklarından üretilebilirse temiz ve yenilenebilir bir döngüye sahiptir. Yapay fotosentez yenilenebilir ve sürdürülebilir yakıtlar için umut verici bir yaklaşım olarak düşünülmektedir. Fotokatalizin çevresel problemlere ve yenilenebilir enerji üretimine büyük katkıda bulunacağı umulmaktadır. Titanya esaslı fotokatalitik materyaller eşsiz kimyasal ve optik özelliklerinden dolayı yapay fotosentez araştırmalarında geniş çaplı olarak kullanılan materyal gruplarından biridir. Hidrojen üretimi için TiO_2 kullanarak fotokatalitik su parçalama, temiz, düşük maliyetli ve çevre dostu hidrojen üretimi için umut verici bir alternatif sunmaktadır.

Bu çalışmada, ZrO_2 katkılı TiO_2 fotokatalitik tozlar birlikte çöktürme ile hazırlandı ve karakterize edildi. Bu ZrO_2 katkılı TiO_2 fotokatalitik tozların UV görünür ışık altında hidrojen üretimindeki fotokatalitik su parçalama aktiviteleri belirlendi. Tozların faz yapıları, katkıların seviyeleri tarafından etkilendi ve 550-700°C aralığındaki ısıl işlem boyunca birincil parçacık boyutları yaklaşık 130 nm'den 500 nm'ye kadar arttı. Maksimum hidrojen verimi, 0.1-0.1mol% ZrO_2-Nd_2O_3 seviyesinde katkılanan 550°C'de ısıl işlem gören tozda yaklaşık 5000 µmol/hr gcat olarak elde edildi. 10 mol%'nin üstünde ZrO_2 katkılı katalizörlerin hidrojen verimleri 1000 µmol/hr gcat'den düşük bulundu.

TABLE OF CONTENTS

LIST OF FIGURES

Figure **Page**

LIST OF TABLES

Table **Page**

CHAPTER 1

INTRODUCTION

1.1. Introduction

Solar energy is one of the best alternatives to supply future energy demand because of its availability, cost effectiveness, accessibility, capacity, and efficiency compared to other renewable energy sources. Solar energy is commonly considered to be a reliable, non-polluting and clean energy source in comparison to other alternatives. Its utilization also does not cause the release of harmful gases (e.g. oxides of C/N/S and/or volatile organic compounds (VOCs)) and particles (e.g. soot, carbon black, metals, and particulate matter (PM)). The flow of solar energy have been elaborately accomplished in and between different parts of a photosynthetic organism (Kabir et al. 2018). Plants harvest energy from sunlight in order to grow in natural photosynthesis process. Oxygen production by the oxidation of water and carbon dioxide reduction to organic compounds occur during this process. This means that the oxidation of water and the reduction of CO_2 are attained with solar energy. Artificial photosynthesis and photoelectrolysis of water using light energy have been investigated worldwide considering natural photosynthesis as a model (Fujishima, Rao, and Tryk 2000).

Photocatalyst materials play an important role in the success of the photocatalytic processes and artificial photosynthesis. Titanium dioxide (TiO_2) has many benefits by virtue of its high chemical stability when exposed to acidic and basic media, nontoxicity, high oxidizing power and low cost. Titanium dioxide (TiO_2) is an excellent photocatalyst with applications in different areas such as self-cleaning surfaces, decomposition of atmospheric pollution and self-sterilization (Castellote and Bengtsson 2011). However, there is a drawback of TiO_2 which is the inability to utilize visible light. The band gap of TiO_2 is about 3.2 eV and it causes only UV light utilization for hydrogen production. The UV light provides nearly 4% of the solar radiation energy in contrast to visible light which provides about 50% of the solar radiation energy. The use of various dopants have been investigated in order to decrease the band gap energy of stable titania phases for more efficient visible light utilization (Ni et al. 2007).

The ionic sizes of Zr^{4+} and Ti^{4+} are very similar which can make substitutional doping relatively easy in composite Ti/Zr oxide structures. This may form new sub electronic states which can enhance light absorption/decrease e-/h+ recombination during the photocatalytic processes although the band-gaps of pure zirconia phases are generally reported to be in the 3.4-5.7 eV range. These composite strucures may also have a high photocorrosion resistance. The preparation of nanostructured zirconia (ZrO_2) doped titania photocatalysts by using chemical coprecipitation techniques were conducted in this study. The effects of zirconia doping extent and the calcination temperature on nanotitania powder photocatalytic water splitting activities were investigated by the determination of the hydrogen yields.

1.2. Global warming and Greenhouse effect

Global warming is a term used for describing the consequences related with the recent accelerating increase in earth surface temperature (both land and water) as well as its atmosphere. The greenhouse effect is closely related with global warming. Global warming is occuring because of the greenhouse effect combined with increased greenhouse gas emissions by human activities The greenhouse gases are the most important components responsible for the climate pattern change. The greenhouse gases involve water vapor (H_2O), carbon dioxide (CO_2), methane (CH_4), nitrous oxide (N_2O) and fluorinated gases including hydrofluorocarbons (HFCs), perfluorocarbons (PFCs) and sulfur hexafluoride (SF6). Global warming is commonly considered to be one of the most important and critical problems of life on Earth (Freije, Hussain, and Salman 2018).

Every year including 2017 has had an average global temperature warmer than the long-term average since 1976. Over the 137-year period since 1880 the global temperature over land increased by an average of 0.18°F (0.10°C) per decade and 0.11°F (0.06°C) per decade over the ocean. The variation of global temperature is schematically shown in Figure 1.1 compared to 1901-2000.

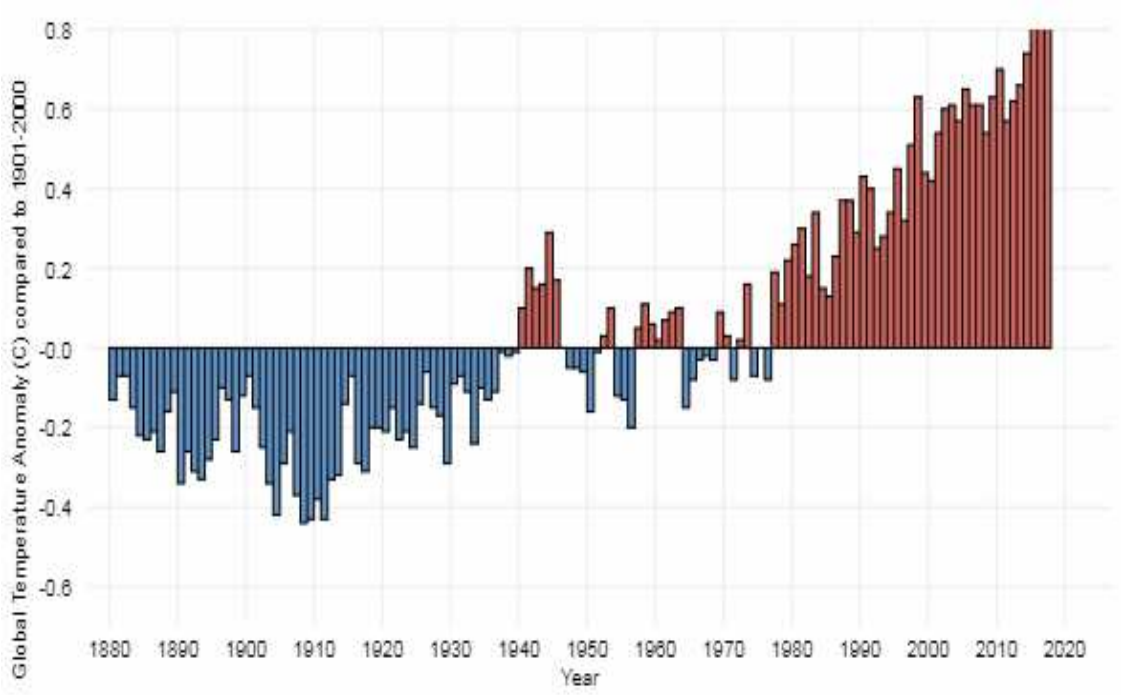

Figure 1. 1. Global temperature anomally vs. year from in the 1880-2018 period. (Source: https://www.ncdc.noaa.gov/)

According to U.S. Energy Information Administration 2018 Report, energy-related CO_2 emissions from the industrial sector will grow the most on both an absolute and relative basis -0.6% annually- from 2017 to 2050 in the Reference case as shown in Figure 1.2. Electric power sector CO_2 emissions are comparatively smooth in the Reference case through 2050 because of the favorable market conditions for natural gas and supportive policies for renewables compared with coal. Natural gas has the largest share of both energy and CO_2 emissions in the industrial sector throughout the projection period. The comparatively low cost of natural gas causes further increases in usage and emissions. Higher energy use of the commercial sector will only slightly be offset by the efficiency gains which is expected to cause emissions increase at a rate of 0.1% annually from 2017 to 2050. CO_2 emissions in the residential and transportation sectors both are expexted to decrease by 0.2%/year over the projection period. Natural gas emissions will increase by an annual rate of 0.8%, while petroleum and coal emissions will decrease at annual rates of 0.3% and 0.2%, respectively. Petroleum emissions will grow in each of the final 13 years of the projection period since increasing vehicle use will outweigh efficiency gains.

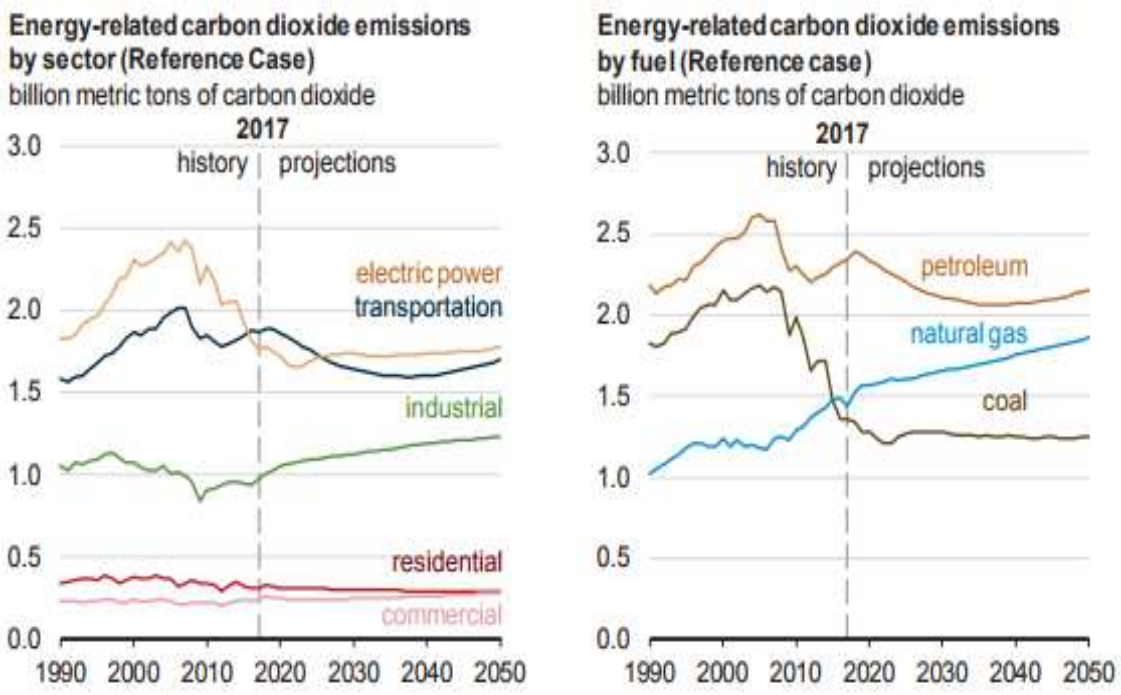

Figure 1. 2. Energy-related carbon dioxide emissions by sector and fuel (Reference case) (Source: Annual Energy Outlook 2018 with projections to 2050)

1.3. Natural and artificial photosynthesis

Solar energy has a great potential as a cheap, clean, renewable and sustainable energy source if it can be captured and transformed into useful forms of energy like plants do since the begining of life on earth. There is an effective approach that is the storage of solar energy in the form of chemical bonds as performed in natural photosynthesis (El-Khouly, El-Mohsnawy, and Fukuzumi 2017). Natural photosynthesis is the process that is conducted by plants, algae and some bacteria which use light energy to split water and further use the generated electrons and hydrogen ions for the reduction of carbon dioxide into sugar. Photosynthesis can be separated into two reactions as the light and the dark reactions which is shown in Figure 1.3. Light strikes Chlorophyll activating electrons to a higher energy state in the light reactions. Light energy is absorbed and used for the synthesis of ATP and reduction of NADP in the light reactions. ATP and NADPH are further consumed in the reduction of carbon dioxide into carbohydrates in the dark reactions (Calvin cycle) (Brotosudarmo et al. 2014).

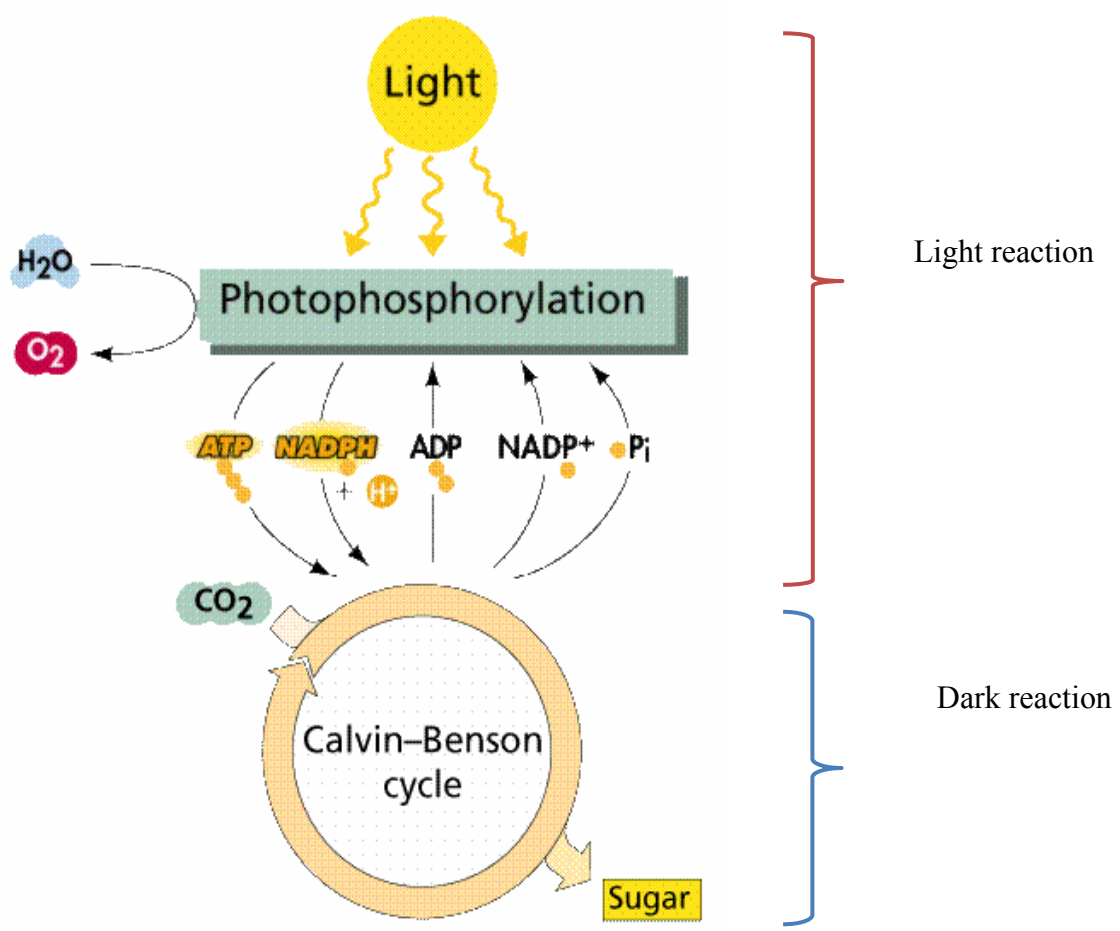

Figure 1. 3. Photosynthesis reaction diagram.
(Source: https://www2.estrellamountain.edu/)

Fuels can be produced from solar energy by both direct and indirect methods. Classification of different methods of solar energy utilization are listed in Figure 1.4 (Mohanta et al. 2015). The fuel is generated in an integrated system in the absence of intermediate energy carriers by the direct method. Artificial photosynthesis represents one of the approaches of producing solar energy by the direct method. Artificial photosynthesis is based on the application of the natural photosynthesis principles on much smaller man-made systems although the basis of artificial photosynthesis is very different from that of the natural photosynthesis process (Hammarstrom and Hammes-Schiffer 2009).

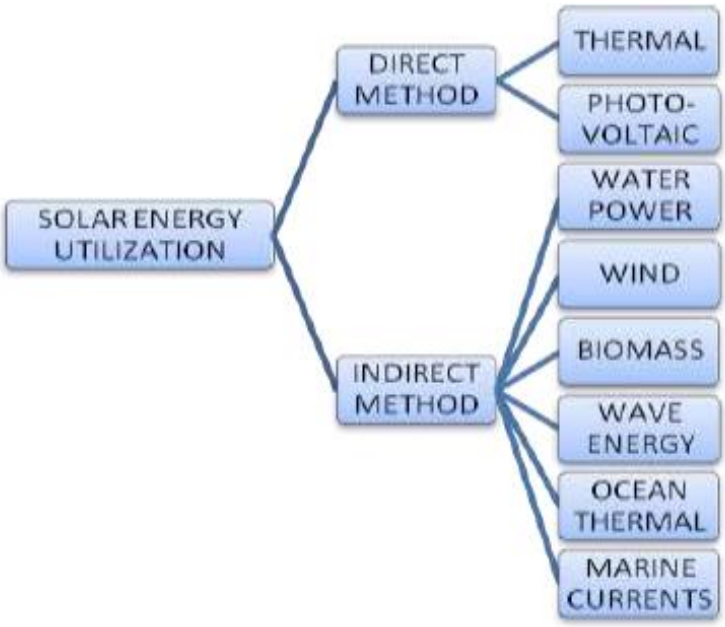

Figure 1. 4. Classification of methods of solar energy utilization.
(Source: Mohanta et al. 2015)

Photosynthesis in green plants have developed over billions of years and is an extraordinarily complex process presenting it an inspiration rather than a model for artificial photosynthesis due its complexity. Honda and Fujishima (Fujishima and Honda 1972) published their pioneering research on light-driven water splitting by direct bandgap excitation of TiO_2 in 1972. Their research findings initiated the publication of intensive research on photoelectrochemical water splitting and solar fuel production based on semiconductors in various liquid junction cell configurations and designs (House et al. 2015).

1.4. Photocatalysts

Photocatalysis is a process that uses a catalyst for accelerating chemical reactions that needs or engages light. A photocatalyst is a semiconductor that can be defined as a substance which is capable of generating electron–hole pairs that provide chemical transformations of the reaction participants, absorbing light and regenerate its chemical composition after each cycle of such interactions. Photocatalytic processes can be separated into two types as homogeneous and heterogeneous photocatalysis (Khan, Adil, and Al-Mayouf 2015). Heterogeneous photocatalysis is a discipline where the

photocatalyst is in a different phase with respect to the substrate (Molinari, Caruso, and Palmisano 2010). Heterogeneous photocatalysis have been widely studied for about three decades since Fujishima and Honda discovered the photocatalytic splitting of water on TiO_2 electrodes in 1972 (Fujishima and Honda 1972).

The ideal photocatalyst should possess the following properties: (Al-Rasheed 2005)

(i) photoactivity
(ii) biological and chemical inertness
(iii) stability toward photocorrosion
(iv) efficiency for solar light activation
(v) low cost
(vi) lack of toxicity

A semiconductor has an electronic structure consisting of a conduction band (CB) and a valence band (VB) that is separated by a bandgap energy (*E*G). An electron is promoted from the VB to the CB with the creation of an electron–hole pair ($e^-_{cb} - h^+_{vb}$) when the photocatalyst is irradiated with photons with energies ($h\upsilon$) equal to or greater than its bandgap as schematically shown in Figure 1.5.

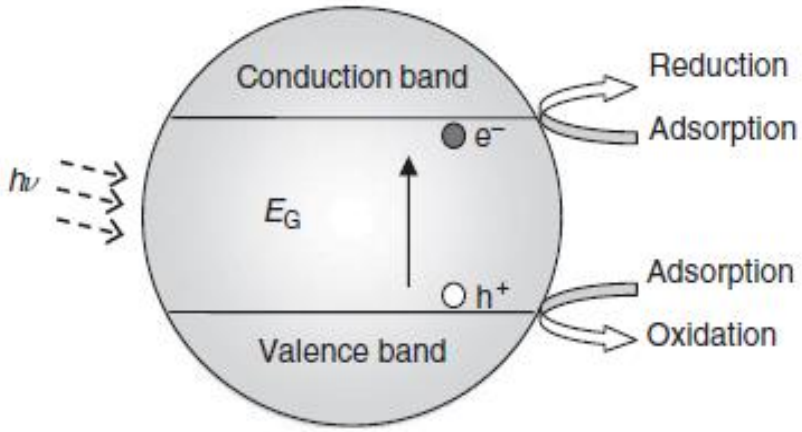

Figure 1. 5. Energy bandgap of semiconductor.
(Source: Molinari, Caruso, and Palmisano 2010)

The mechanism of overall water splitting on a semiconductor particle is schematically showed in Figure 1.6. Electrons (e^-) in the valence band are excited and

jump to the conduction band in the first of step of the process. The holes (h^+) left in the valence band results in the formation of e^- and h^+ pairs if the semiconductor photocatalyst is exposed to radiation with an energy equivalent to or greater than its band gap energy. The photogenerated e^- and h^+ pair are able to reduce and oxidize chemical species on the surface of the photocatalyst, respectively after the above very first step. The original structure (or chemical composition) of the photocatalyst remains unchanged when equal numbers of the photogenerated e^- and h^+ are consumed by the chemical reaction and/or recombination. The bottom of the photocatalyst conduction band must be more negative than the redox potential of H^+ to H_2 (0 V vs. NHE (normal hydrogen electrode) at pH 0) and the top of the valence band must be more positive than the oxidation potential of H_2O to O_2 (1.23 V vs. NHE (normal hydrogen electrode)) (Nguyen and Wu 2018) in order to accomplish photocatalytic water splitting . Band gap energies of oxide photocatalysts and non-oxide photocatalysts are given in Figure 1.7. The valence and conduction bands of oxide photocatalysts are affected by changes in the pH whereas pH changes has almost no effect the on the valance and conduction bands of non-oxide photocatalysts which constitutes the major difference between these two types of photocatalysts (Byrne, Subramanian, and Pillai 2017).

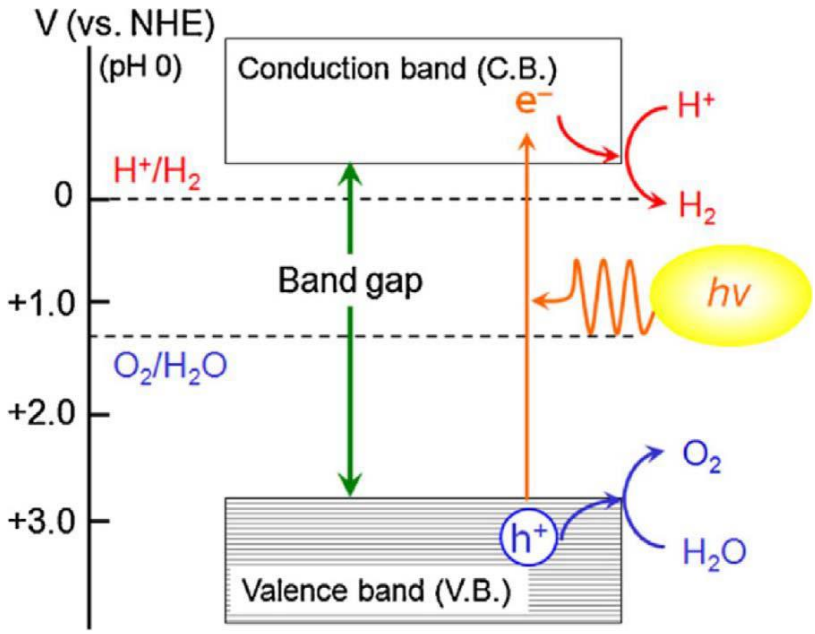

Figure 1. 6. Basic mechanism of overall water splitting on a semiconductor particle. (Source: Nguyen and Wu 2018)

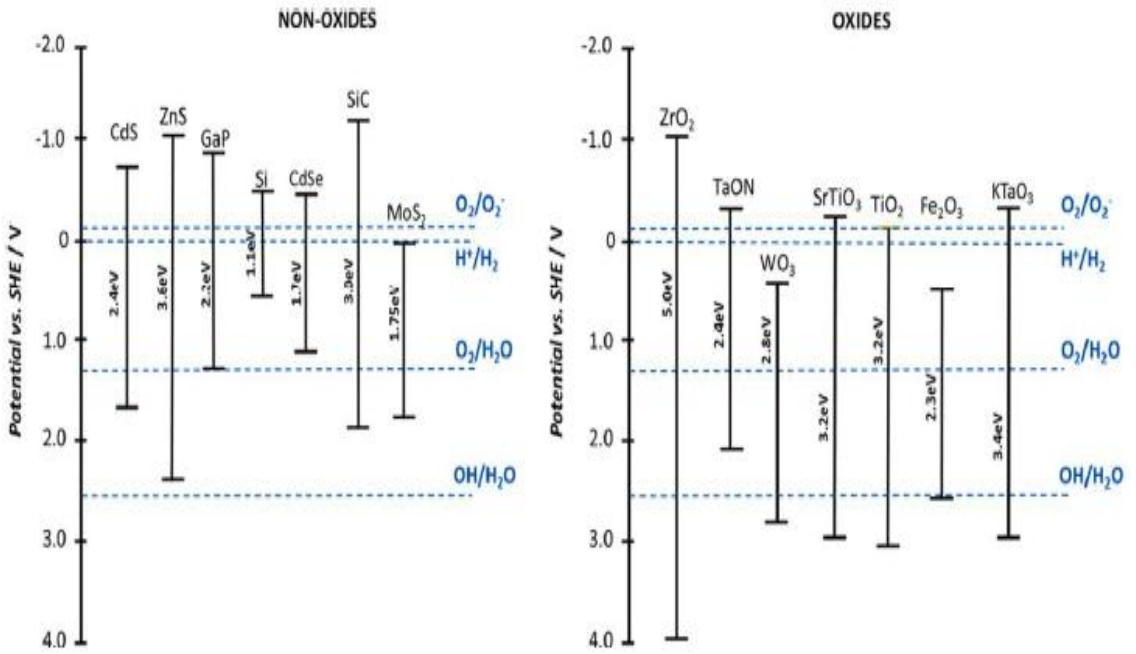

Figure 1. 7. The band gaps of non-oxide photocatalysts (left) and oxide photocatalysts at a pH of 7 (right). (Source: Byrne, Subramanian, and Pillai 2017)

Research on heterogeneous photocatalysis intensified rapidly after the discovery of the photocatalytic water splitting by Fujishima and Honda. Research conducted by Fujishima and Honda was focussed on the use of this new concept in energy storage and renewable energy generation (Fujishima and Honda 1972). Applications have been developed in various other areas such as environmental cleaning, drinking water treatment, industrial, and health applications in recent years besides the initial intended energy related areas (Al-Rasheed 2005). A large number of publications indicates that photocatalysis is a sustainable technology and it has low cost for the treatment of a host of pollutants in air and water including organics and heavy metals, *etc*. Photocatalysis is being carried out worldwide because the use of sunlight or UV radiation presents an inexpensive environmentally friendly choice of technologies and the extent of this global interest is shown in Figure 1.8 in the form of publication numbers since the pioneering introduction of the concept in the 1970s.

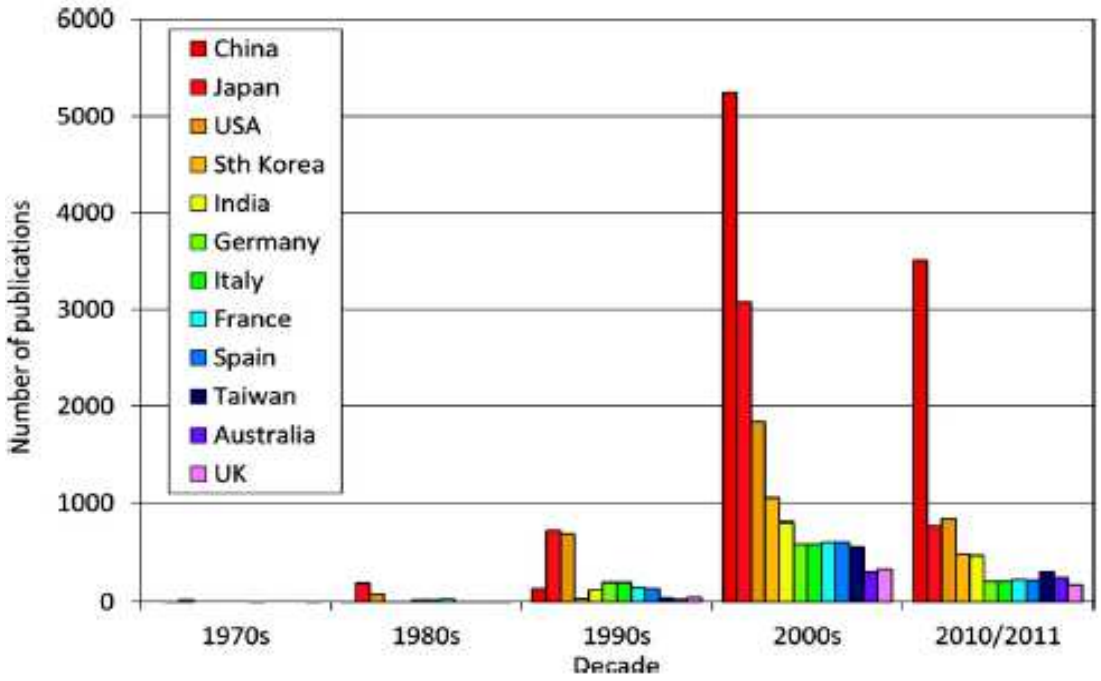

Figure 1. 8. Number of publications pertaining to photocatalysis since 1970. (Source: Ibhadon and Fitzpatrick 2013)

Many types of semiconductors consisting of various oxides, sulfides and nitrides capable of being used for photocatalysis are presently known. TiO_2 (Eg = 3.2 eV), WO_3 (Eg = 2.8 eV), $SrTiO_3$ (Eg = 3.2 eV), α-Fe_2O_3 (Eg = 3.1 eV) ZnO (Eg = 3.2 eV), ZnS (Eg = 3.6 eV), CuO (Eg = 1.2 eV), CdS (Eg = 2.4 eV), CdSe (Eg = 1.7 eV) and GaN (Eg = 3.4 eV) can be listed as some of these materials along with their band-gap energies (Hoffmann et al. 1995). Intensive research have indicated that because of its suitability, low cost, biological and chemical inertness, stability with respect to photocorrosion and chemical corrosion, TiO_2 is used in many environmental applications as a photocatalyst.

UV photocatalysts and visible light active photocatalysts are used for hydrogen production by water splitting. TiO_2 and titanates, Nb- and Ta- based oxides, W-, Mo-, and V-based oxides, d^{10} Metal oxide photocatalysts, f^0 Metal oxide photocatalysts, nonoxide photocatalysts are commonly used UV photocatalysts. Current research on visible light active photocatalysts is concentrated on various topics like efficient separation of photogenerated charge carriers, cocatalyst loading, Z-scheme photocatalysts, metal sulfides, GaN:ZnO solid solution photocatalysts, and electron mediators (Ismail and Bahnemann 2014).

1.5. Titanium dioxide (Titania, TiO_2)

Titania has been known for a long time and is a commonly known familiar material which is currently used in food colouring, toothpastes, cosmetics and white pigments in paints. TiO_2 have been widely used because of its strong optical absorption, high chemical stability, nontoxicity and low cost in scientific studies on photocatalysis, photovoltaic cells, photodegradation, electrochromic devices *etc.* after the first study by Fujishima and Honda (Fujishima and Honda 1972) about photocatalytic splitting of water on a TiO_2 electrode under ultraviolet (UV) light in 1972 (Yin et al. 2013).

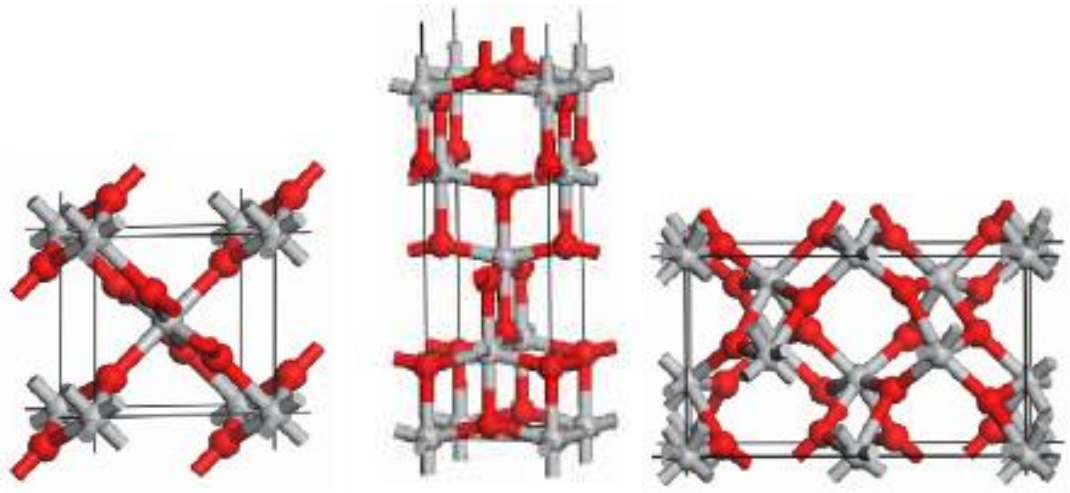

Figure 1. 9. Bulk crystal structure of rutile, anatase and brookite (from left to right). Titanium atoms are gray, and oxygen atoms are red. (Source: Woodley and Catlow 2009)

There are eight phases of titanium dioxide (titania) which are anatase, rutile, brookite, baddeleyite, columbite, pyrite, cotunnite and fluourite. The final five titania phases (columbite, baddeleyite, pyrite, fluourite and cotunnite) can be formed at very high temperatures and/or pressures. Anatase, rutile and brookite phases are thermodynamically more stable than the other titania phases and their crystal structures are shown in Figure 1.9 and their bulk properties are further tabulated in Table 1.1. The titania phases except

anatase and rutile have an indirect gap which causes the lack of photocatalytic activity (Sigmund et al. 2009).

Table 1. 1. Bulk properties of TiO_2

(Source: Sigmund et al. 2009 and Diebold 2003)

Crystal structure	System	Space group	Lattice constants (A°)			density (kg/m^3)
			a	b	c	
rutile	tetragonal	D^{14}_{4h}-$P4_2/mnm$	4.578	4.578	2.953	4240
anatase	tetragonal	D^{19}_{4h}-$I4_1/amd$	3.782	3.782	9.502	3830
brookite	tetragonal	D^{15}_{2h}-Pbca	5.436	9.166	5.135	4170

The demand for TiO_2 has been exceedingly increased due to the use of TiO_2 in many applications. TiO_2 is commonly produced by using several methods such as: sulfate method, chloride method (vapor method), alkoxide method and specific methods for industrial applications (Shon et al. 2009). These methods have differences related with the starting titanium precursor used and the involved reaction mechanisms. The alkoxide, sulfate chloride, sol-gel and chemical precipitation methods are described briefly below.

Sulfate method

In sulfate method, titanium oxysulphate ($TiOSO_4$) which is formed by dissolving titanium minerals in sulfuric acid is treated with a base to form hydrated TiO_2. After heat treatment (calcination) crystalline TiO_2 powders are obtained. Hydrated TiO_2 synthesized by sulfate method has low photocatalytic activity since it has crystal defects which act as centers for recombination of electron-hole pairs despite the high surface area. The calcined hydrated TiO_2 has also low photocatalytic activity because of the contaminants (sulfate ion or ions from minerals) originating from the method.

Chloride method

This method is also called as vapor method because titanium minerals are reacted with chlorine gas yielding titanium tetrachloride ($TiCl_4$) and oxidized to TiO_2 at 700-1000^oC. Crystallization of TiO_2 into anatase or rutile also occurs because of the application of high temperatures. Commercially available Degussa P-25 which is commonly used by researchers is synthesized by using this method. Degussa P-25 has 80 wt.% anatase and 20 wt.% rutile phases and has a very high photocatalytic activity under UV illumination.

Alkoxide method (Sol-Gel)

Metal alkoxides are mostly used precursors for metal oxide synthesis in laboratory scale since the product of sulfate method has contaminations and chlorine method reaction conditions are hard to control. Also metal alkoxide can be produced in highly pure grade which leads to highly pure metal oxide. TiO_2 can be synthesized from various titanium alkoxides (e.g. titanium ethoxide, titanium propoxide, titanium butoxide). Titanium alkoxide is hydrolysed to form TiO_2 sol/precipitate. TiO_2 sol is then gelated to form polymeric TiO_2. Proper heat treatment of TiO_2 gels leads to highly active TiO_2 with high specific surface areas. This method is known as the "Sol-gel" method in the literature. The main reactions in sol-gel processing of titanium alkoxides are given below:

Hydrolysis reactions;

$$M(OR)_4 + H_2O \rightarrow HO\text{-}M(OR)_3 + R\text{-}OH \text{ (partial hydrolysis)}$$
$$M(OR)_4 + 2H_2O \rightarrow (OR)_2\text{–}M\text{-}(OH)_2 + 2R\text{-}OH \text{ (partial hydrolysis)}$$
$$M(OR)_4 + 3H_2O \rightarrow (OR)\text{–}M\text{-}(OH)_3 + 3R\text{-}OH \text{ (partial hydrolysis)}$$
$$M(OR)_4 + 4H_2O \rightarrow M(OH)_4 + 4R\text{-}OH \text{ (total hydrolysis)}$$

Condensation reactions;

$$(OR)_3\text{–}M\text{-}OH + HO\text{–}M\text{-}(OR)_3 \rightarrow [(OR)_3M\text{–}O\text{–}M(OR)_3] + H\text{-}O\text{-}H$$
$$(OR)_3\text{–}M\text{-}OR + HO\text{–}M\text{-}(OR)_3 \rightarrow [(OR)_3M\text{–}O\text{–}M(OR)_3] + R\text{-}OH$$

Sol-gel method has several advantages such as high purity and homogenous product, low temperature synthesis, excellent atomic mixing, precise control of size and surface properties, wide variety of precursors or other chemicals, possibility of different form of products such as films or powders. High amount of solvent usage in this method makes it unfeasible for the high production rates of TiO_2.

Chemical precipitation

Chemical precipitation is a liquid phase reaction which is used to synthesize insoluble solid particles. Solid particles obtained during precipitation, the precipitate, are formed in the solution due to a reaction or when the solution has been supersaturated by a compound. Titanium precipitates as titanium hydroxide ($Ti(OH)_4$), TiO_2 or titanium oxy hydroxide ($TiO(OH)_3$). Titanium precursor can be alkoxide based or inorganic (e.g. $TiCl_4$). The dissolved precursor solution is mostly precipitated by the use of an alkali solution since Ti^{4+} is soluble in acidic conditions. The precipitates can be crystalline or amorphous particles. Rare earths mostly precipitate as hydroxides in aqueaous media. Crystalline oxide/hydroxide nanoparticles are synthesized by the application of heat treatment to the as-precipitated hydroxide particles. Usually an aqueous or alcohol solution of inorganic salt (nitrate, chloride, sulfate) of the desired rare earth is reacted with an alkali solution (of NaOH, NH_4OH) in this method. However unwanted growth of particles is inevitable during calcination. Direct precipitation from a non-aqueous solution should be carried out in order to obtain ultrafine particles (2-5 nm)(Yurtsever, H.A., PhD Thesis, 2015).

CHAPTER 2

LITERATURE SURVEY

2.1. Photocatalytic Water Splitting Activities of TiO_2 Based Materials in Hydrogen Production

Photoelectrochemical hydrogen production by using TiO_2 was firstly reported by Fujishima and Honda (Fujishima and Honda 1972). They also investigated the use of different photocatalysts such as TiO_2, ZnO, CdS, GaP, WO_3 and SiC for water splitting. A large number of research papers have been published on this topic in the last couple of decades since their pioneering work.

Recent research have shown that titanium dioxide (TiO_2) stays as being one of the most valuable photocatalysts for H_2 generation due to its favourable properties such as low-cost and environmentally friendly clean hydrogen production capacity by using solar energy when compared with other photocatalysts. Noble metal loading, addition of sacrificial reagents and dye sensitization as alternative catalyst modification methods also are the subject of current research (Fujishima, Rao, and Tryk 2000, Khan, Adil, and Al-Mayouf 2015, Lan, Lu, and Ren 2013, Ni et al. 2007)

Reddy et al. (2003) investigated the effect of the physicochemical properties of ZrO_2 prepared by different hydrolyzing agents such as NH_4OH, KOH and urea (NH_2CONH_2) on the photocatalytic activity for water splitting based on characteristic methods. A reference ZrO_2 were obtained by the calcination of $Zr(OH)_4$. Zirconium hydroxide powders were precipitated from zirconium oxychloride solutions by using three different hydrolyzing agents [NH_4OH, KOH and urea (NH_2CONH_2)]. The hydroxide precipitates were calcinated at 750°C for 6 h after dring at 120°C. The powder surface areas and crystal structures differed significantly with preparation method as determined by the conducted characterization studies. The ZrO_2 powder with the highest surface area prepared by using KOH as the hydrolyzing agent was determined to have the highest photocatalytic activity. Photocatalytic activity increased by a factor of 2-3 with the addition of Na_2CO_3 to pure water. The hydrogen and oxygen production capacities

along with the crystal structures of the powders are given in Table 2.1 (R. Reddy, Hwang, and Lee 2003).

Table 2. 1. The crystal structure and the photocatalytic activity of ZrO_2. (Source: R. Reddy, Hwang, and Lee 2003)

Catalyst	Crystal structure (%)		Photocatalytic activity (μmol/gcat.h)[a]			
			Pure water		Na_2CO_3 solution	
	Monoclinic	Tetragonal	H_2	O_2	H_2	O_2
Standard-ZrO_2	95	5	60	32	142	72
ZrO_2 (KOH)	56	44	112	55	296	150
ZrO_2 (NH_4OH)	78	22	72	38	180	92
ZrO_2 (Urea)	82	18	95	48	214	110

[a]Catalyst 0.3 g; distilled water 500 ml; inner irradiation-type reaction cell made of quartz, 450 W high-pressure Hg lamp, Na_2CO_3 80 g.

Kokporka et al. (2013) investigated the effect of molar ratios, calcination time and temperatures in the 500°C to 900°C range on the photocatalytic activities of ZrO_2 doped TiO_2 powders. Powders were prepared by using sol-gel method. The specific hydrogen production rate was determined to be the highest for the powder with a 95:5 molar ratio due to the increase in the specific surface area of the photocatalyst which causes the formation of more available active sites as given in Figure 2.1.

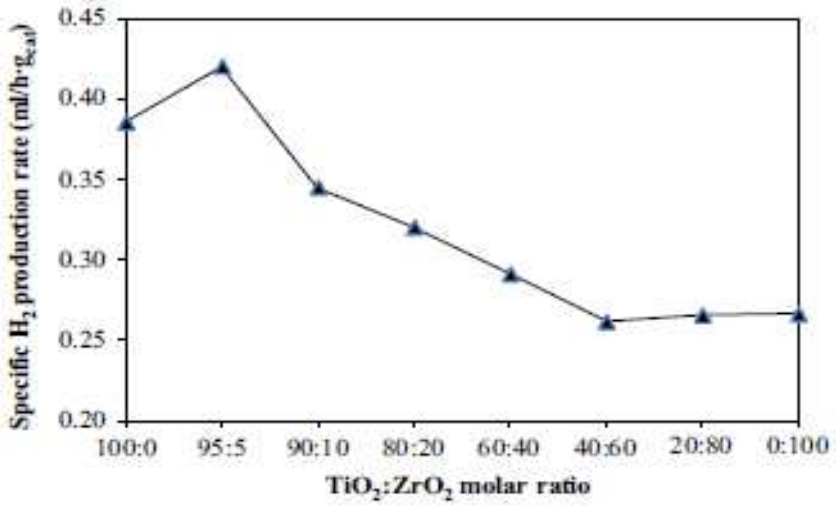

Figure 2. 1. Effect of TiO_2-to-ZrO_2 molar ratio on the specific rate of hydrogen production using the synthesized TiO_2–ZrO_2 mixed oxide photocatalysts calcined at 500°C for 4 h (photocatalyst, 0.2 g; total reaction solution volume, 150ml; DEA concentration, 15 vol.%; EY concentration, 0.1mM; initial solution pH, 11.6; irradiation time,5 h). DEA=diethanolamine; EY=Eosin Y. (Source: Kokporka et al. 2013).

The calcination time did not significantly effect the specific hydrogen production activities of the photocatalysts as shown Figure 2.2. A 4 h calcination time was choosen in order to complete the crystal structure development under any conditions in this study.

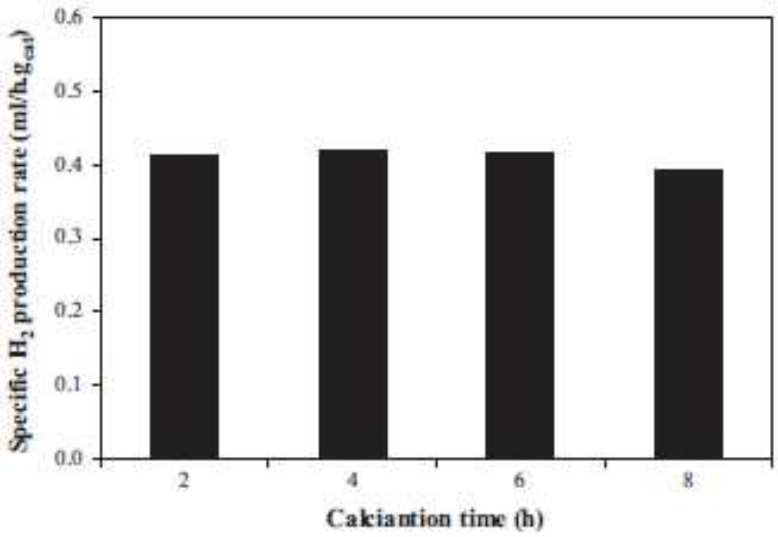

Figure 2. 2. Effect of calcination time on the specific rate of hydrogen production using the synthesized $0.95TiO_2$–$0.05ZrO_2$ mixed oxide photocatalyst calcined at 500°C (photocatalyst, 0.2 g; total reaction solution volume, 150 ml; DEA concentration, 15 vol.%; EY concentration, 0.1 mM; initial solution pH, 11.6; irradiation time, 5 h). DEA= diethanolamine; EY=Eosin Y. (Source: Kokporka et al. 2013).

Figure 2.3a reveals that the highest photocatalytic hydrogen production activity of pure TiO_2 was determined at the optimum calcination temperature of 500°C and it maintained a specific hydrogen production rate of 0.38 ml/hgcat. Photocatalyst specific surface area decreased and the anatase-to-rutile phase transformation occurred when calcination temperature was increased. The photocatalytic hydrogen production capacity of the $0.95TiO_2$–$0.05ZrO_2$ mixed oxide increased with increasing calcination temperature up to 800°C in contrary to pure TiO_2. A maximum specific hydrogen production rate of 0.61 ml/h gcat was obtained at 800°C. Photocatalytic activity was decreased and the anatase-to-rutile phase transformation occurred when calcination temperature was increased to 900°C. The enhancement percentages plotted in Figure 2.3b indicates that calcination of the $0.95TiO_2$–$0.05ZrO_2$ mixed oxide nanocrystal photocatalyst at 800°C was the most appropriate for the highest specific H_2 production rate. The specific H_2 production rate enhancement declined rapidly when anatase-to-rutile phase transformation occured.

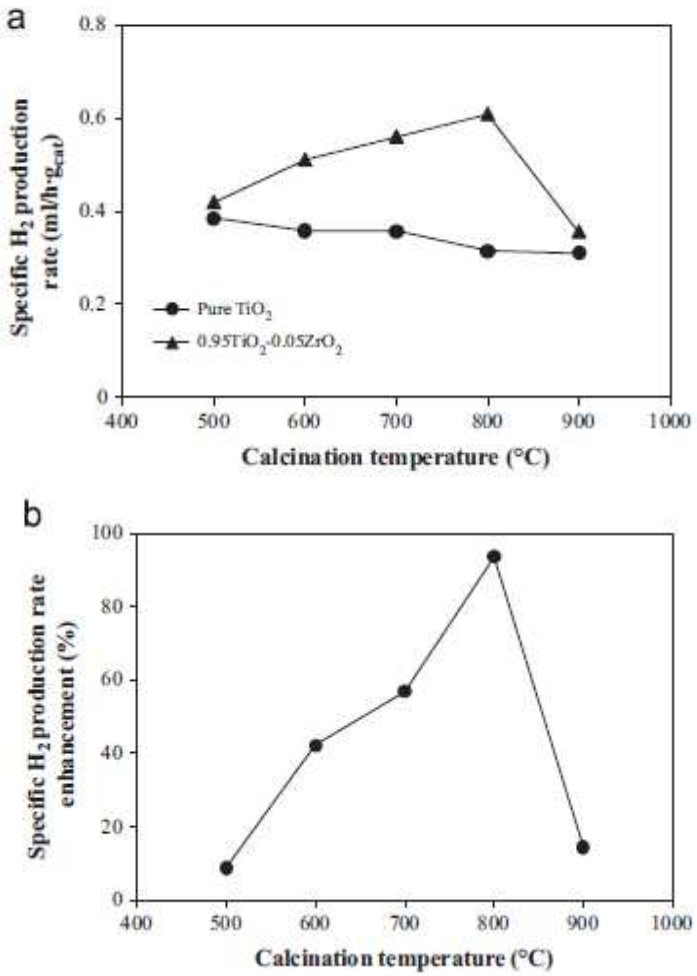

Figure 2. 3. Effect of calcination temperature on (a) the specific rate of hydrogen production using the synthesized pure TiO_2 and 0.95TiO_2–0.05ZrO_2 mixed oxide photocatalysts and (b) enhancement of the specific hydrogen production rate (photocatalyst, 0.2 g; total reaction solution volume, 150 ml; DEA concentration, 15 vol.%; EY concentration, 0.1 mM; initial solution pH, 11.6; irradiation time, 5 h). (Source: Kokporka et al. 2013).

Zhang et al. (2017) investigated the photocatalytic activity of a series of gully-like TiO_2–ZrO_2 composites with various molar ratios such as pure TiO_2, pure ZrO_2, 1:0.25, 1:1, 1:2 and 1:4. The band gap of TZ (TiO_2-ZrO_2) 1:0.25 was comparatively small among all TZ samples that show better activity in the photocatalytic degradation of organic pollutants because of its promising light absorption performance as shown in Figure 2.4b. The gully width of gully-like composites such as TiO_2, TZ 1:0.25, TZ 1:1, TZ 1:2 and TZ 1:4 were nearly 1.70, 2.06, 2.10, 2.35 and 0.89 mm, respectively as tabulated in Table 2.2. The addition of ZrO_2 led to an initial increase of the gully width till TZ 1:2 and was reduced with further zirconia addition.

Table 2. 2. The BET surface area (S_{BET}), average pore diameter (D), pore volume (Vtotal), band gap energy (Eg), and gully width (W) of TiO_2, ZrO_2 and the gully-like TiO_2–ZrO_2 composites. (Source: Zhang et al. 2017)

Sample	$S_{BET}/(m^2\ g^{-1})$	D/nm	$V_{total}/(cm^3\ g^{-1})$	E_g/eV	W/μm
TiO_2	125.1	4.5	0.16	3.15	1.70
ZrO_2	130.4	3.7	0.07	3.41	—
TZ 1:0.25	75.1	3.6	0.15	3.08	2.06
TZ 1:1	121.5	2.0	0.16	3.16	2.10
TZ 1:2	140.9	1.9	0.14	3.26	2.35
TZ 1:4	88.6	1.7	0.16	3.32	0.89

The photocatalytic H_2 production capacity of the samples increased with ZrO_2 content as shown in Figure 2.4e. The evolved hydrogen yield of 0.1 g of TZ 1:4 attained 97.1 μmol g^{-1} in 8h and it had a more suitable capacity of water photolysis.

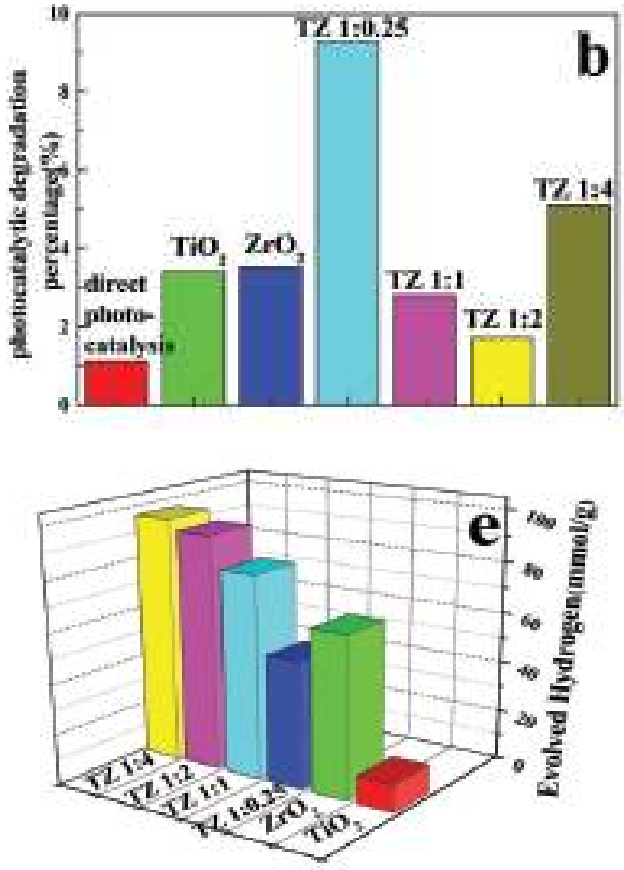

Figure 2. 4. (b) The results of solar light photocatalytic degradation (t = 240 min) for MO profiles with different photocatalysts; (e) Experimental results of photocatalytic H_2 evolution from different catalysts. (Source: Zhang et al. 2017)

Zhu et al. (2016) prepared Pt/HS-TiO_2 hollow spheres and determined their water-splitting activities under visible-light irradiation. Pt/HS-TiO_2 was prepared by sol-gel method. 1.0 wt% Pt loading as a cocatalyst provided the highest H_2 generation rate of 1023.71 $\mu molh^{-1}g^{-1}$ when compared with 0.5 wt% Pt/HS-TiO_2, 1.5 Pt/HS-TiO_2 and HS-TiO_2 photocatalysts. The HS-TiO_2 powder with no cocatalyst had the lowest hydrogen yield of about 4.56 $\mu molh^{-1}g^{-1}$ as shown in Figure 2.5.

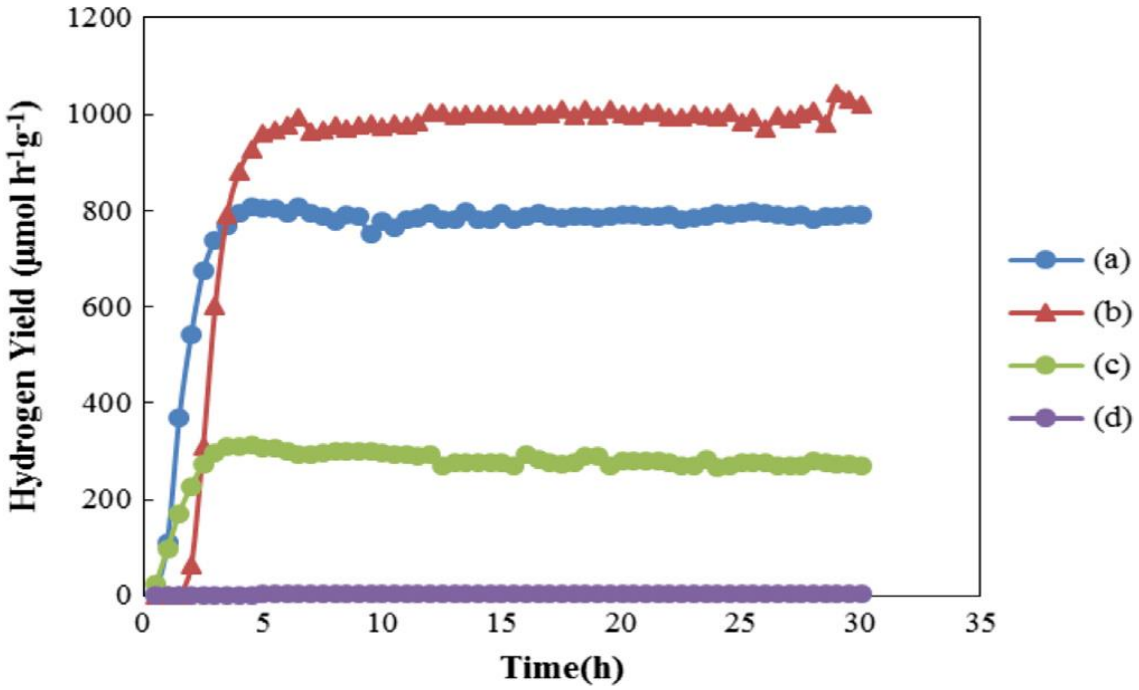

Figure 2. 5. Photocatalytic H_2 evolution amount vs.visible light (λ>400 nm) irradiation time by using (a) 0.5 wt% Pt/HS-TiO2, (b)1.0wt%Pt/HS-TiO_2, (c)1.5wt%Pt/HS-TiO_2 and (d)HS-TiO_2. (Source: Zhu et al. 2016)

There were no critical changes in the original hydrogen productivity for 1.0 wt% Pt/HS-TiO_2 after 35 days. The 1.0 wt% Pt/HS-TiO_2 powder was concluded to represent a photocatalyst alternative with a long-life and a good reusability/stability as shown in Figure 2.6.

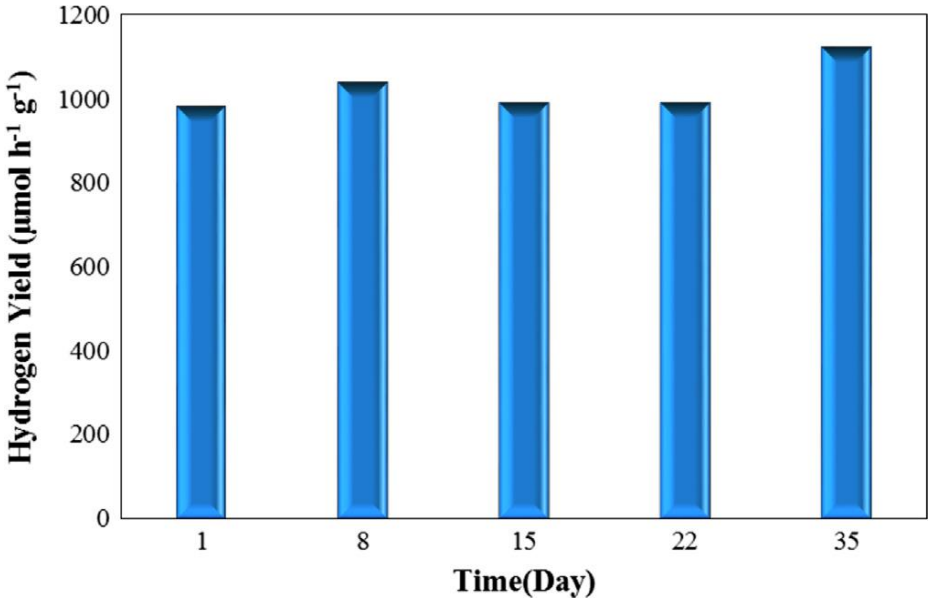

Figure 2. 6. The reuse of 1.0 wt% Pt/HS-TiO_2 photocatalytic H_2 evolution by water splitting at room temperature.(Source: Zhu et al. 2016)

Onsuratoom, Chavadej, and Sreethawong (2011) investigated the effect of TiO_2-ZrO_2 molar ratio, calcination temperature, photocatalyst type and Ag loading on the water splitting/hydrogen production capacities of mixed oxide photocatalysts. The surface area of ZrO_2-loaded photocatalysts were higher than unloaded TiO_2 at a calcination temparature of 500°C. This is due to the decrease in the photocatalyst grain size by the addition of a second metal oxide leading to an increase in the specific surface area. The surface area decreased with the increase in the calcination temperature in the 500°C-700°C range due to pore collapse. Ag loading increased the specific surface area of the $0.93TiO_2$-$0.07ZrO_2$ mixed oxide photocatalyst heat treated at 500°C. The addition of ZrO_2 restricted grain growth and decreased crystallite size in the photocatalyst microstructure. The crystallite sizes of pure TiO_2 and $0.93TiO_2$-$0.07ZrO_2$ mixed oxide photocatalyst were increased with the calcination temperature in the 500°C to 750°C range. The Ag dispersion results of the Ag-loaded mesoporous assembled $0.93TiO_2$-$0.07ZrO_2$ mixed oxide photocatalyst calcined at 500°C indicated that Ag dispersion was increased at 0.5 wt.% (59.8%) and then started to decrease. The specific hydrogen production rate increased by nearly 2.5 times at $0.93TiO_2$-$0.07ZrO_2$ mixed oxide photocatalyst compared to pure TiO_2 as seen in Figure 2.7. The specific hydrogen production rate decreased due to the high band gap energy of ZrO_2 (5eV) although the

specific surface area of the TiO_2-ZrO_2 mixed oxide was higher above 7 mol% zirconia doping.

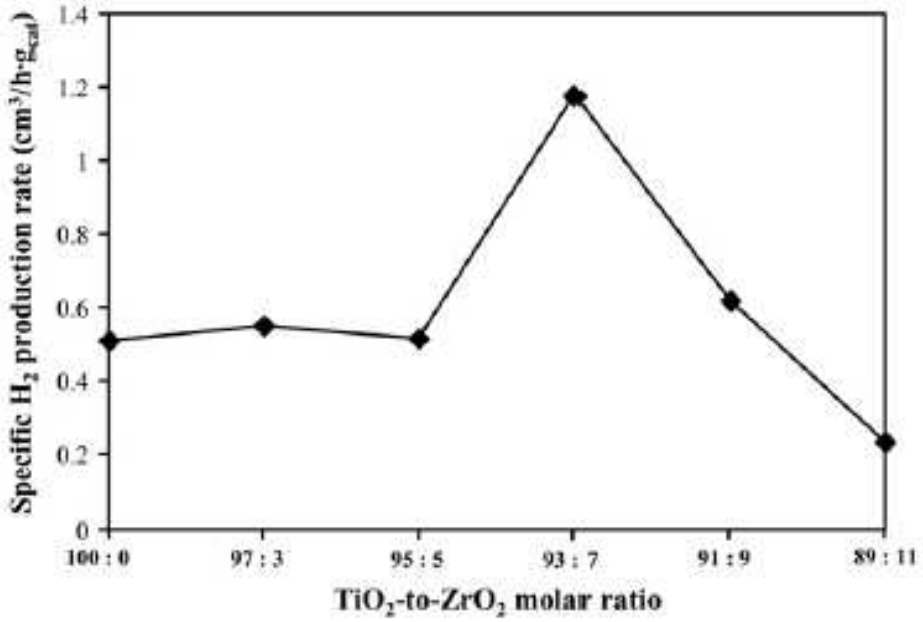

Figure 2. 7. Effect of TiO_2-to-ZrO_2 molar ratio on specific H_2 production rate over the synthesized mesoporous assembled TiO_2-ZrO_2 mixed oxide photocatalysts calcined at 500°C (Photocatalyst, 0.2 g; total volume, 200 ml containing distilled water 100 ml and methanol 100 ml; and UV irradiation time, 5 h). (Source: Onsuratoom, Chavadej, and Sreethawong 2011)

Various commercial photocatalysts such as P-25 TiO_2, JRC-01 TiO_2, and JRC-03 TiO_2 showed lower specific hydrogen production performances than $0.93TiO_2$-$0.07ZrO_2$ mixed oxide photocatalyst. The specific hydrogen production rate of pure TiO_2 and $0.93TiO_2$-$0.07ZrO_2$ mixed oxide at different calcination temperatures indicated that the hydrogen production activity had an optimum value at 500°C. The activity decreased due to the specific surface area reduction of both photocatalysts with increasing calcination temperature as shown in Figure 2.8.

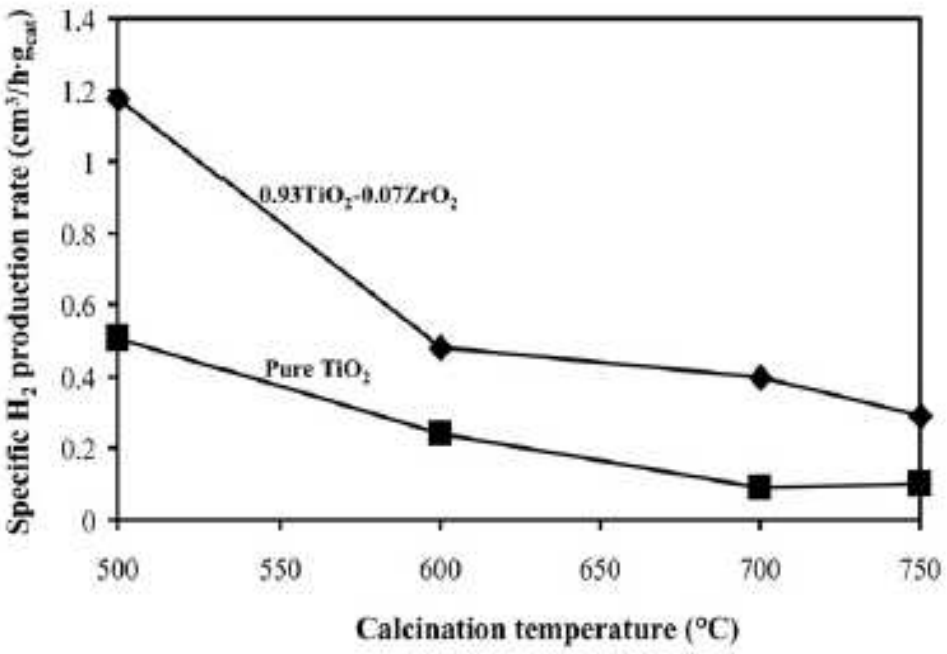

Figure 2. 8. Effect of calcination temperature on specific H_2 production rate over the synthesized mesoporous assembled pure TiO_2 and $0.93TiO_2$-$0.07ZrO_2$ mixed oxide photocatalysts (Photocatalyst, 0.2 g; total volume, 200 ml containing distilled water 100 ml and methanol 100 ml; and UV irradiation time, 5 h). (Source: Onsuratoom, Chavadej, and Sreethawong 2011)

2.2. The Photocatalytic Activity Enhancement of TiO_2 via Different Methods

Hassan et al. (2012) investigated and characterized the rare earth doped (Ln^{3+}–TiO_2, Ln = La, Ce and Nd) TiO_2 nanofibers prepared by the sol–gel electrospinning method. The photocatalytic activity of the samples was determined by dye degradation under UV light irradiation. The XRD analysis indicated that all samples were in anatase phase at 500 °C. The rutile phase contents of all samples was increased with calcination temperature up to 700°C. The optical absorption edges of the Ln^{3+}–TiO_2 samples shifted to higher wavelengths with dopant due to the charge-transfer transition between rare earth ions and host TiO_2. Nd^{3+}-TiO_2 photocatalyst had the highest absorption edge wavelength as shown in Figure 2.9.

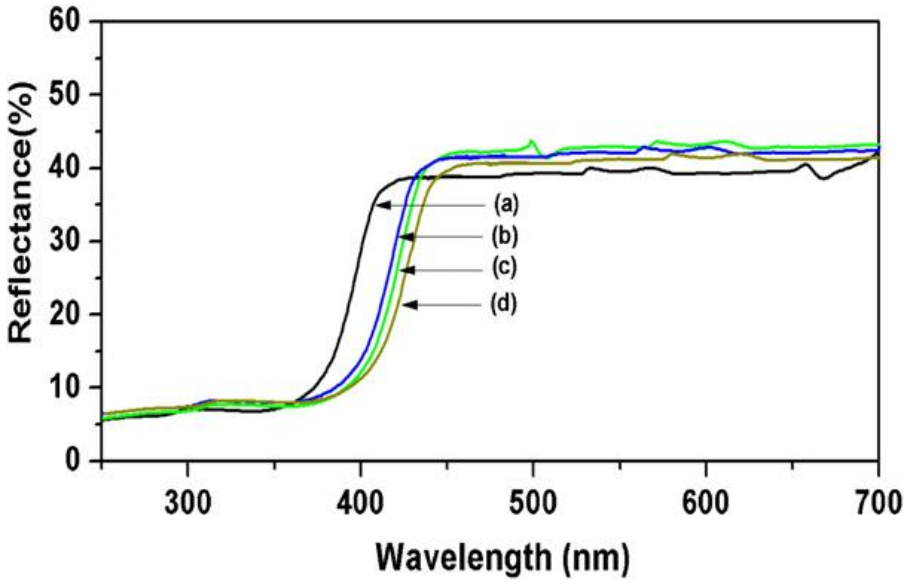

Figure 2. 9. UV–vis DRS spectra of (a) TiO_2, (b) La–TiO_2, (c) Ce–TiO_2, and (d) Nd–TiO_2 nanofibers. (Source: Hassan et al. 2012)

The surface characteristics, crystallinity, absorption and other nanofiber properties reveals that the photocatalytic degradation of pure TiO_2 was enhanced by rare earth doping. Nd^{3+}-TiO_2 photocatalyst had a higher photocatalytic activity than other rare earth doped nanofibers as shown in Figure 2.10.

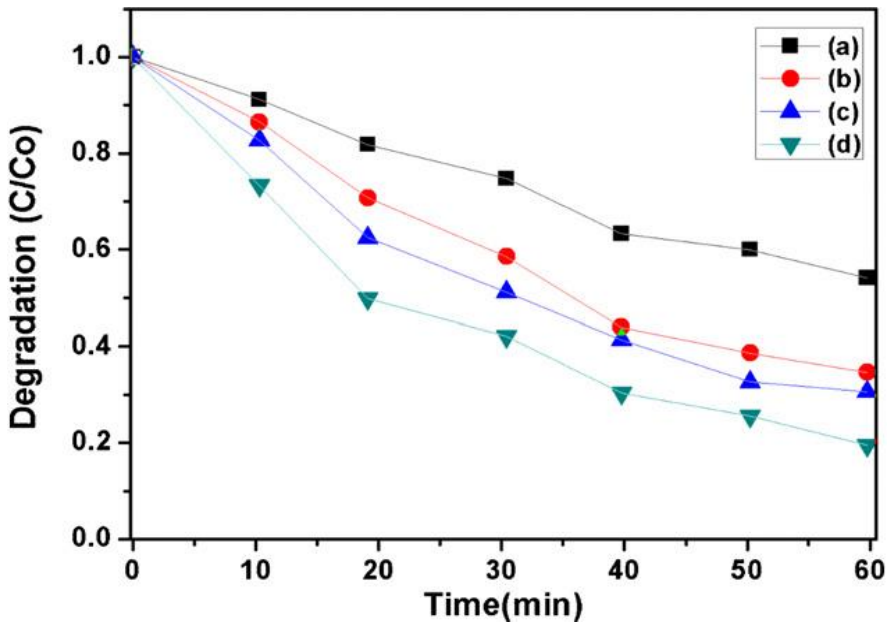

Figure 2. 10. Photocatalytic degradation of R6G over the different rare earth-doped TiO_2 catalysts (a) TiO_2, (b) La–TiO_2, (c) Ce–TiO_2, and (d) Nd–TiO_2 nanofibers with the same doped contents (1.0 wt%). (Source: Hassan et al. 2012)

Onsuratoom, Puangpetch, and Chavadej (2011) investigated the photocatalytic hydrogen production activity of the mesoporous-assembled $0.93TiO_2$–$0.07ZrO_2$ mixed oxide photocatalysts synthesized by sol-gel process which were doped with non-precious metals like Ag, Ni, and Cu. All of the samples had very narrow and uniform pore size distributions. Agglomerated clusters were formed by the aggregation of several uniform-sized photocatalyst nanoparticles as was observed from SEM images. The specific surface area of the $0.93TiO_2$–$0.07ZrO_2$ mixed oxide photocatalysts were enhanced slightly with various metal loading. The specific surface area decreased at higher metal loadings for each metal type (i.e. at 0.5 wt.% Ag, 0.5 wt.% Ni, and 0.15 wt.% Cu) above a maximum value. The crystallite sizes of the mixed oxides were slightly affected by metal loading as obtained from XRD analysis. Cu-loaded photocatalyst possessed higher UV light absorption than Ni-loaded and Ag-loaded photocatalyst. Ag-loading increased the band gap energy of the mesoporous-assembled 0.93TiO2–0.07ZrO2 mixed oxide photocatalyst nanoparticles due to the decreased absorption onset wavelength as compared to Ni-loaded and Cu-loaded photocatalysts. The photocatalytic hydrogen production activity of the mesoporous-assembled $0.93TiO_2$–$0.07ZrO_2$ mixed oxide photocatalysts increased significantly by Ag, Ni, and Cu loading as seen in Figure 2.11. That was attributed to the Schottky barrier stimulation in the mixed oxides with metal nanoparticle loading which relatively eases the electron transfer to the metal active sites to stimulate the photocatalytic hydrogen production. The 0.15 wt.% Cu-loaded $0.93TiO_2$–$0.07ZrO_2$ mixed oxide photocatalyst showed the highest photocatalytic hydrogen production activity with a hydrogen production rate of 12.8 $cm^3\,h^{-1}$ gcat which was followed by Ni and Ag loadings respectively. The photocatalytic activity for each metal type increased with metal dispersion for all metals. The higher electronegativity observed for the Cu-loaded photocatalyst led to the formation of more active sites which increased photocatalytic hydrogen production activity. The Cu-loaded $0.93TiO_2$–$0.07ZrO_2$ mixed oxide was concluded to be the most efficient photocatalyst due to its physical, chemical, and electrochemical properties.

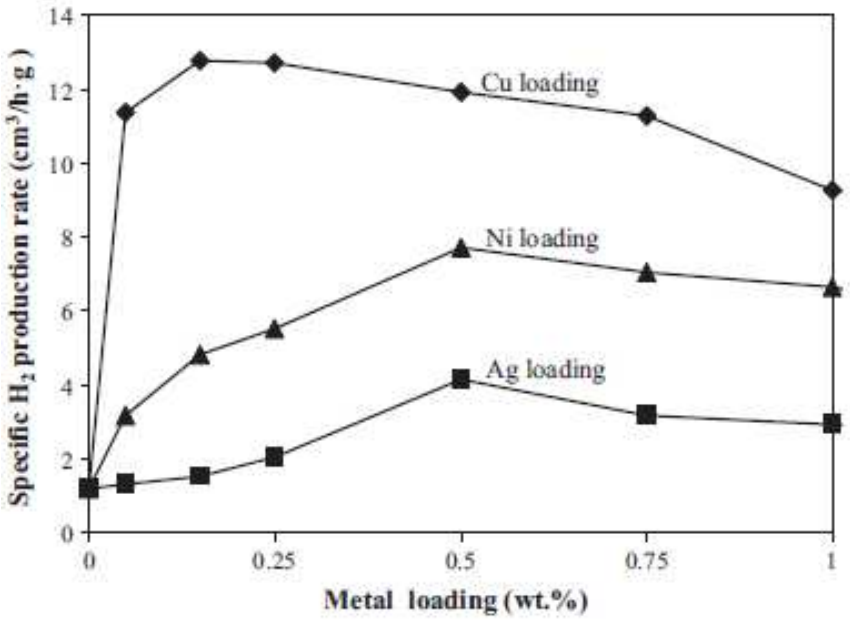

Figure 2. 11. Effect of metal loading on specific H_2 production rate over the synthesized metal-loaded mesoporous-assembled $0.93TiO_2$–$0.07ZrO_2$ mixed oxide photocatalysts (Photocatalyst, 0.2 g; total volume, 200 ml containing distilled water 100 ml and methanol 100 ml; and UV irradiation time, 5 h). (Source: Onsuratoom, Puangpetch, and Chavadej 2011)

Pliekhov et al. (2017) investigated the effect of carbon and/or zirconium co-modification on the photocatalytic activity of TiO_2. TiO_2 was synthesized with a sol-gel hydrothermal based technique. The photocatalytic activity of the samples were analyzed by using the degradation of methylene blue (MB) in aqueous solution under ultraviolet and visible light irradiation and their results are presented in Figures 2.12 and 2.13. XRD results have shown that anatase was the dominant phase all samples. The crystallite sizes of Zr and/or C modified TiO_2 were smaller than pure TiO_2 since doping carbon and/or zirconium could supply disparate boundaries resulting in a barrier for the growth of TiO_2 crystals. DLS analysis indicated that TiO_2-Zr,C sample possessed the smallest agglomerated clusters that provided the largest surface area of 128 m^2g^{-1}. The absorbance of the TiO_2-C and TiO_2-Zr-C samples in the visible light region of the spectra was higher than TiO_2-Zr and TiO_2 samples due to the absoption of visible light by C. The band gap energy of carbon modified TiO_2-Zr sample was narrow in comparison with TiO_2-Zr sample since carbon eliminated the negative influence of zirconia.

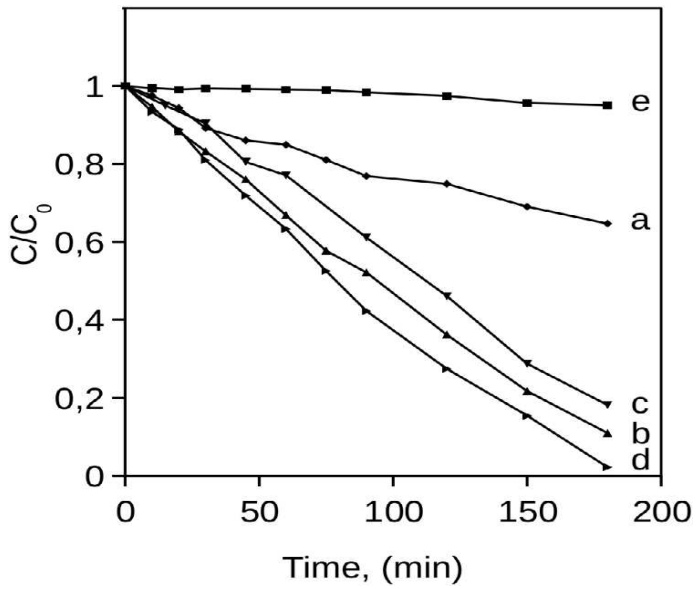

Figure 2. 12. Decomposition of methylene blue under UV-A light irradiation shown by the change in absorption at 664 nm after different times in the presence of various photocatalysts: a) TiO_2, b) TiO_2Zr, c) TiO_2C, d) TiO_2Zr,C, e) Blank. (Source: Pliekhov et al. (2017)

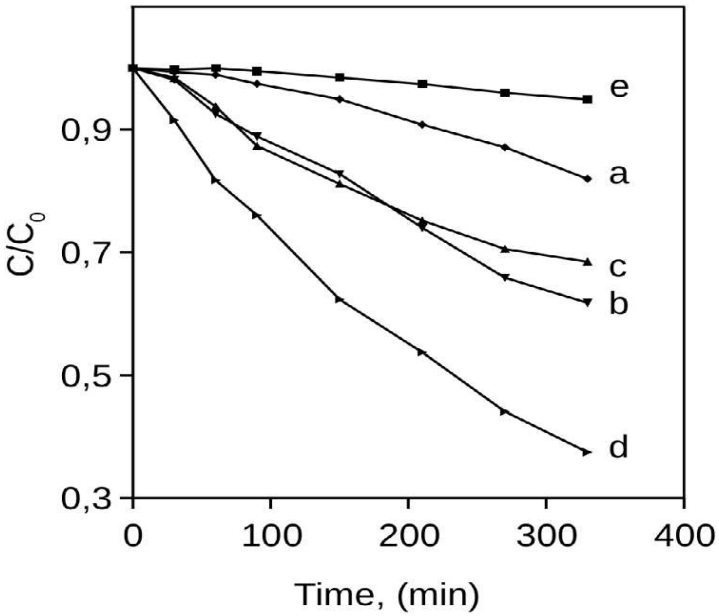

Figure 2. 13. Decomposition of methylene blue under visible light irradiation shown by the change in absorption at 664 nm after different times in the presence of variousphotocatalysts: a) TiO_2, b) TiO_2Zr, c) TiO_2C, d) TiO_2Zr,C, e) Blank. (Source: Pliekhov et al. 2017)

The modification of TiO_2 sample with both zirconium and carbon indicated methylene blue (MB) degradation values of 97% and 63%, respectively with the ultraviolet light driven and visible driven photocatalytic processes as seen in Figure 2.12

and Figure 2.13. They were the best results among all samples since the surface acidity was enhanced by doping of TiO_2 with both Zr and C. Active sites on the TiO_2 surface were discussed to be possibly created by Zr doping and substitution of surface lattice titanium atoms with carbon.

CHAPTER 3

MATERIALS AND METHODS

3.1. Materials

Titanium tetraisopropoxide (TTIP, Aldrich 97%) as the titanium precursor, neodymium nitrate hexahdrate [$Nd(NO_3)_3.6H_2O$, Aldrich 99.9% trace metal basis], ammonium hydroxide (NH_4OH), zirconium(IV) propoxide (ZTP, Aldrich 70%) as dopant precursor and ethanol (Absolute Merck) were used for the preparation of the photocatalyst powders in this work. Copper (II) nitrate [$Cu(NO_3)_2.2.5H_2O$ Aldrich 99.9% trace metal basis], methanol -sacrificial organic species- (Merck, absolute) were used in the photocatalytic water splitting experiments.

3.2. Preparation of the Photocatalytic Powders

The synthesis of the undoped and doped TiO_2 photocatalysts were performed by using a chemical coprecipitation method in alcoholic media. The synthesis was conducted by the dropwise addition of TTIP/ethanol (1.6M) solution into the NH_4OH/ethanol solution (0.65M) under constant stirring for the preparation of the undoped TiO_2 photocatalyst. A white precursor precipitate was obtained at the end of the synthesis. The precipitate suspension was filtered through a Buchner Funnel and washed with ethanol. The filter cake was dried in an oven at 70 ^oC overnight.

Zirconia(ZrO_2) and Zirconia(ZrO_2)-Neodymium(Nd_2O_3) doped TiO_2 photocatalysts were prepared by the same chemical procedure. Powders were doped at a series of preselected ZrO_2 molar contents as follows :0.1%, 1%, 5%, 10%, 50% (oxide based molar composition of the respective cations Zr and Ti) and 0.1-0.1 mol% ZrO_2-Nd_2O_3. The difference between the preparation of undoped and doped photocatalysts was the dropwise addition of TTIP/ZTP/ethanol solution into the NH_4OH/ethanol solution and NH_4OH/NdNitrateHexahydrate/ethanol solution for 0.1-0.1 mol% ZrO_2-Nd_2O_3 doped powder precipitation. The filtered precipitates were dried at 70°C overnight and

calcinated at 550, 575, 600, 625, 650 or 700°C for 3 hours. Photocatalyst powder preparation and characterization process is schematically shown in Figure 3.1.

3.3. Characterization of the Powders

Phase characterization of the prepared powders was performed by Philips X'pert Pro XRD equipment with monochromated high-intensity λ=1.54Å CuKα radiation. The scanning rate was 2.5 2Θ/min between 5° and 80° with 0.033° step size.

The powder morphology/size was determined by scanning electron microscopy (SEM FEI QUANTA 250 FEG). All samples were coated by Au in order to increase the conductivity. The powder DLS (Dynamic Light Scattering) particle size distributions were obtained by using Malvern NanoZS90.

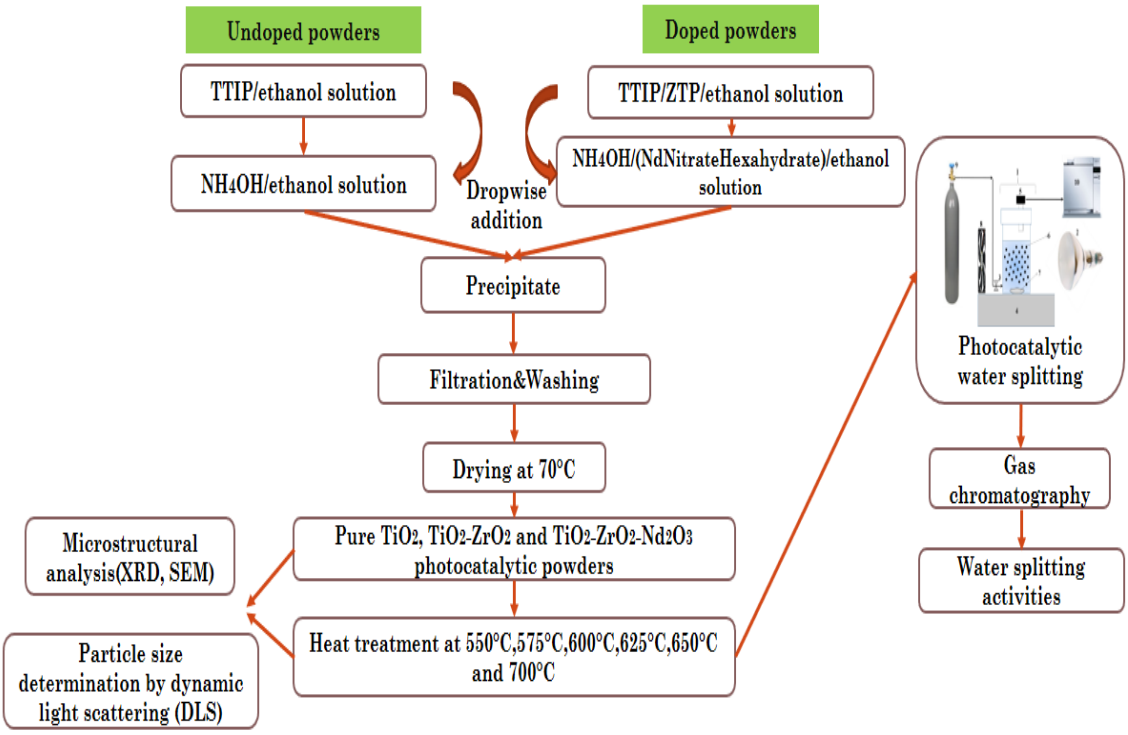

Figure 3. 1. Flow diagram of photocatalytic powder preparation and characterization process.

3.4. Photocatalytic Water Splitting Setup

Photocatalytic hydrogen production experiments were performed with in-situ copper (Cu) photodeposition. Copper was deposited or formed as a co-catalyst in the titanium dioxide system since copper a promising catalyst for photoreforming due to its cheapness and abundance in the Earth's crust. Copper-TiO_2 based photocatalysts have been prepared by using metal Cu, CuO, Cu_2O, $Cu(OH)_2$, and CuS, alone or in presence of a second co-catalyst in recent research papers. Copper deposition on the TiO_2 surface have been shown to decrease the band gap of TiO_2 by producing either active trap centers for electrons or through the formation of surface structural defects. Moreover, it was observed that the use of sacrifical organic species (alcohols and organic acids) increased the hydrogen production rate due to the quick oxidation reaction with positive holes which also accelerates photogenerated electron proton ion reduction reactions (Clarizia et al. 2016). The copper deposition and sacrificial organic species reactions involving e_{CB}^- and h_{VB}^+ are as follows:

- The reduction of cupric ions by photogenerated electrons:

$$Cu(II) + e_{CB}^- \rightarrow Cu(I) + e_{CB}^- \rightarrow Cu(0) \quad (3.1)$$

- The oxidation of the sacrificial organic species by photogenerated positive holes:

$$S_{ads} + h_{VB}^+ \rightarrow S_{ox} + H^+ \quad (3.2)$$

In-situ Cu photodeposition was performed according to the following procedure. Stock solution of Cu^{2+} was first prepared by dissolving copper (II) nitrate ($Cu(NO_3)_2.2.5H_2O$ Aldrich 99.9% trace metal basis) in deionized water at room temperature with a concentration of $1.79x10^{-4}$ g Cu/mL. Required amounts of Cu stock solution and methanol -sacrificial organic species- (Merck, absolute) were mixed in a 100 ml volumetric flask. 0.15 g of TiO_2 powder was added into the schott glass bottle and Cu stock solution/methanol mixture were subsequently added. TiO_2 powders were dispersed through mechanical mixing in the final solution (100 mL, 25 % v/v methanol-water) prior

to UV-Vis irradiation. Simulateneous hydrogen production was observed and quantified by a gas chromatograph (Agilent Technologies 7820A GC System) during in-situ Cu photodeposition process. A schematic illustration of Cu photodeposition mechanism is shown in Figure 3.2.

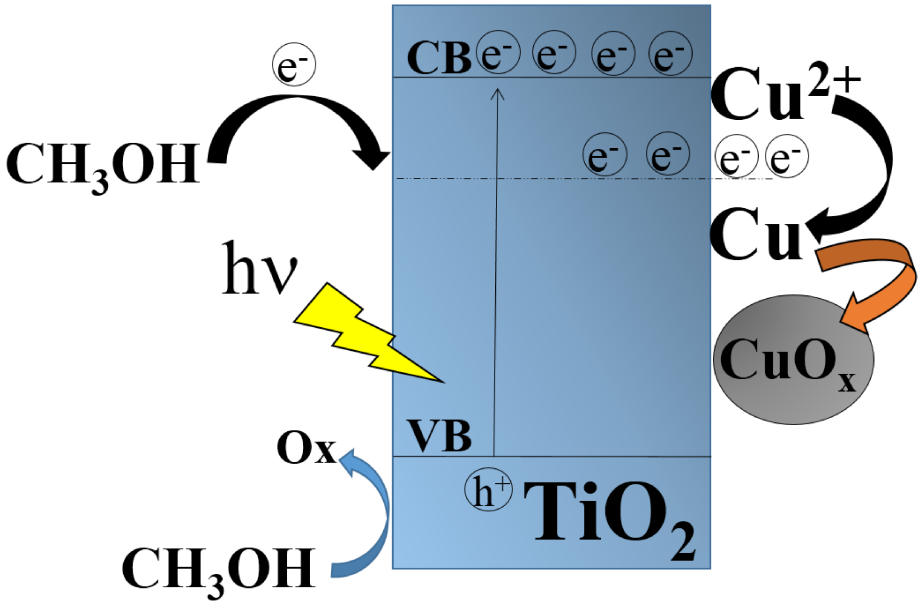

Figure 3. 2. Schematic illustration of copper photodeposition mechanism.

The photocatalytic water splitting process was carried out in a homemade Pyrex photoreactor with N_2 (99.99%) source for initial purging. Photocatalytic water splitting was determined and quantified by Agilent 7820A (Gas Chromatograph-GC) equipped with a Molecular Sieve 5A column and thermal conductivity detector (TCD). He (High purity, 99.99%) carrier gas volumetric flow rate was 20 mL/min and pressure was 4 bar. Back inlet, oven and back detector temperatures were 200°C, 105°C and 250°C, respectively.

Photocatalytic water splitting experiments were performed simultaneously with in-situ Cu photodeposition (by GC quantification). The 100 mL volumetric flask of Cu stock solution (2094 µL)/methanol (25 mL)/water (15 mL) solution were added into the photoreactor that was 133 mL, liquid and gas volumes were 100 mL and 33 mL, respectively. The undoped and doped photocatalysts were dispersed by a magnetic stirrer

throughout the experiment to avoid mass transfer limitations and to hold the photocatalyst particles suspended. Before the photocatalytic reaction, the photoreactor was purged with N_2 gas bubbling for 15 minutes while the UV-Vis lamp (Osram Ultravitalux 300W) is off in order to avoid the undesired reaction between dissolved oxygen and photogenerated electrons and to keep anaerobe conditions in the photoreactor. The photocatalytic reaction was started by subjecting the mixture to UV-Vis lamp. After the visible light irradiation, 1 mL of sample was extracted by using a syringe through the GC sampling valve for every 15 minutes in 3 hours throughout the experiment. The gas samples were analyzed by gas chromatography. The set up is as shown in Figure 3.3. The stepwise progress of the water splitting process in the form of pictures is further shown in Figure 3.4.

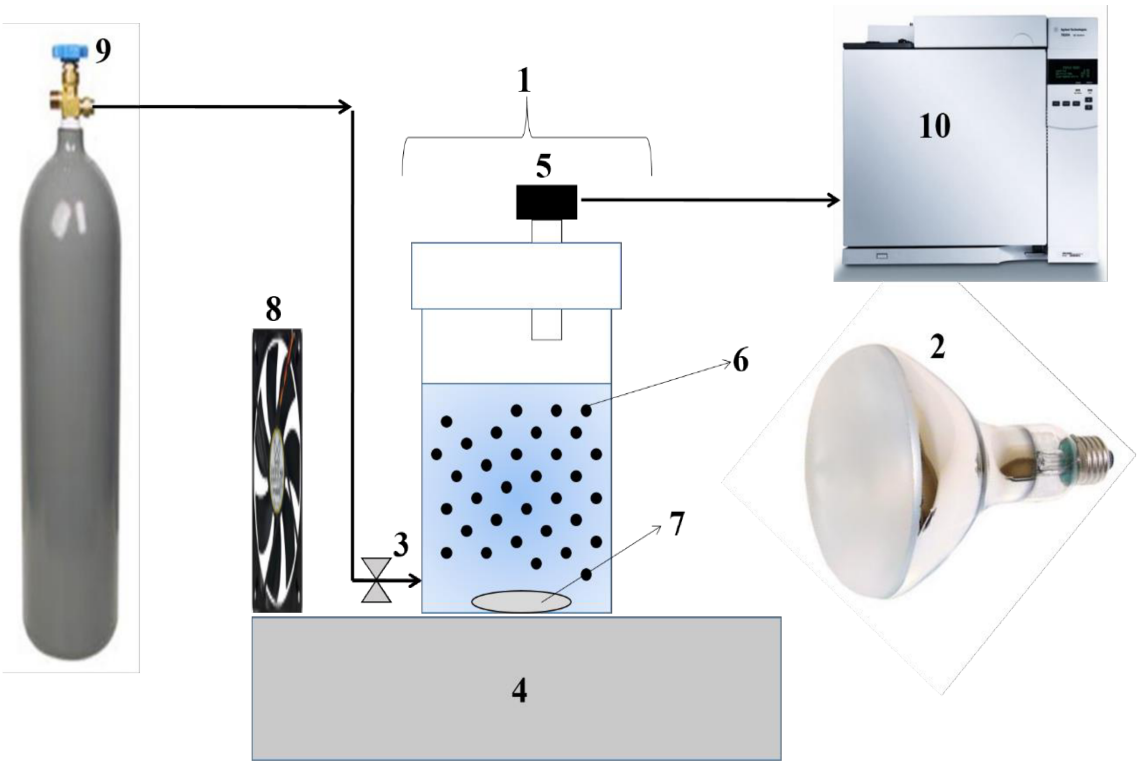

Figure 3. 3. Photocatalytic water splitting setup. 1: Photoreactor, 2: UV-Vis lamp (Osram Ultravitalux 300W), 3: N_2 inlet, 4: Magnetic stirrer, 5: Gas outlet, 6: Photocatalyst particles, 7: Magnetic bar, 8: Cooling fan, 9: N_2 source, 10: Gas Chromatograph.

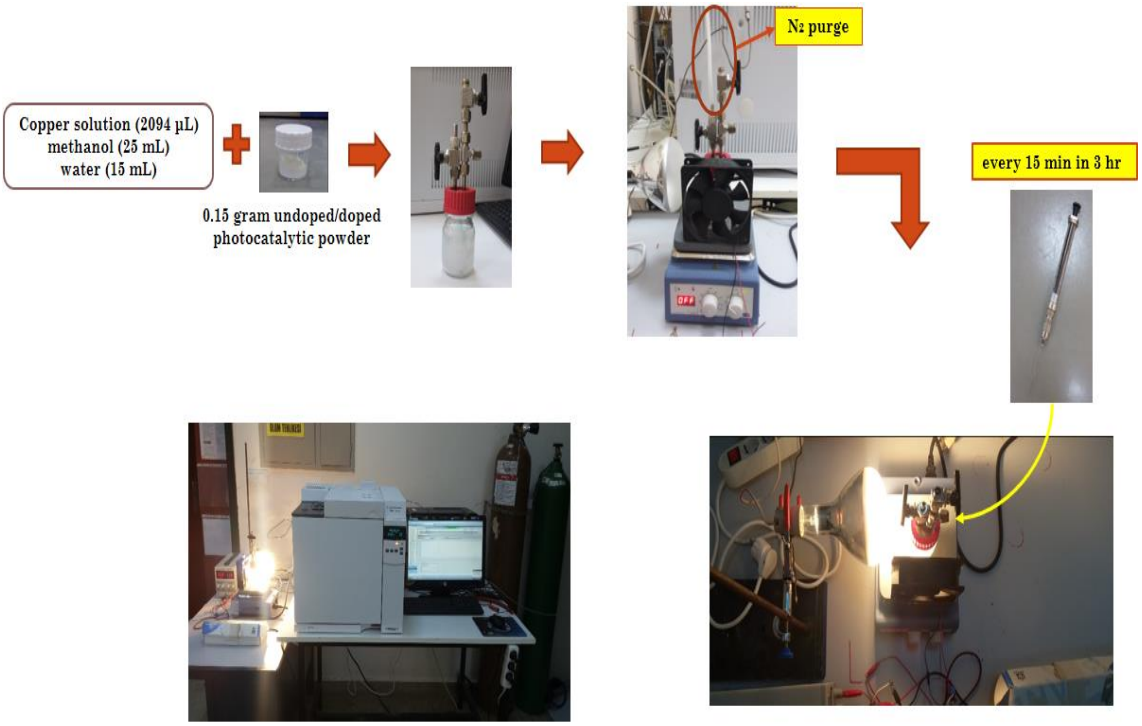

Figure 3. 4. Photocatalytic water splitting process.

CHAPTER 4

RESULTS AND DISCUSSION

4.1. Characterization of the Powders

The evolution of photocatalyst powder primary particles and their aggregation/agglomeration during processing is schematically shown in Figure 4.1. The primary particles form almost instantly upon the introduction and mixing of the alkoxide contaning drops to the vigorously mixed precipitant solution through fast hydrolysis/condensation reactions. These primary particles may be amorphous and/or crystalline but evolve during heat treatment and are probably formed from 5-10 nm crystallites. Aggregates and agglomerates which are bigger in size are formed from primary particles coprecipitation and/or further pocessing like filtration/drying/heat treatment. Relatively stronger solid bridges may be present in between the primary particles in aggregates whereas weaker bonds bring the primary particles/aggregates in agglomerates. The morphology is most likely dictated by the supersaturation levels and rate of mixing during particle coprecipitation.

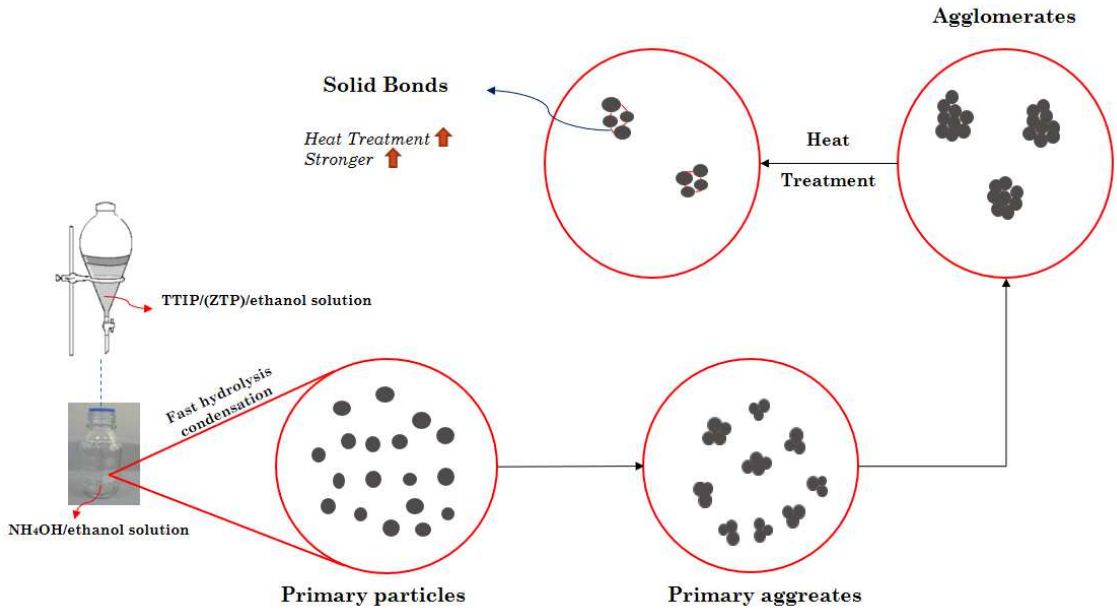

Figure 4. 1. The morphology of photocatalytic powders.

The SEM images of 0.1-0.1 mol% ZrO_2-Nd_2O_3 doped TiO_2 photocatalytic powders as precipitated and dried at 70 °C, heat treated at 550°C, 575°C, 600°C, 650°C and 700°C at 100 kX magnification is given in Figures 4.2 - 4.7. The presence of nanosized primary particles can be clearly seen in these images. The primary particles in the dried powders before heat treatment have a uniaxial/spherical morphology with sizes heavily in the 100-150 nm range along with a lower number of bigger particles. These primary particles form primary aggreagates which are about 3-5 times bigger in size. These aggregates form bigger entities during precipitation/drying which are commonly known as agglomerates with much bigger particle sizes.

The primary particle morphology of the heat treated photocatalyst powders are similar to the dried precursor powder morphology. The sizes of the primary particles are about similar to the precursor powder particles after heat treatment at 550°C as can be seen in Figure 4.3. The sizes of the primary particles increase gradually with heat treatment temperature up to about 500 nm at 700°C. The primary aggregates present in the precursor densified to form these relatively bigger particles at high heat treatment temperatures along with significant neck formations in between the primary particles (most easily detected in Figure 4.4).

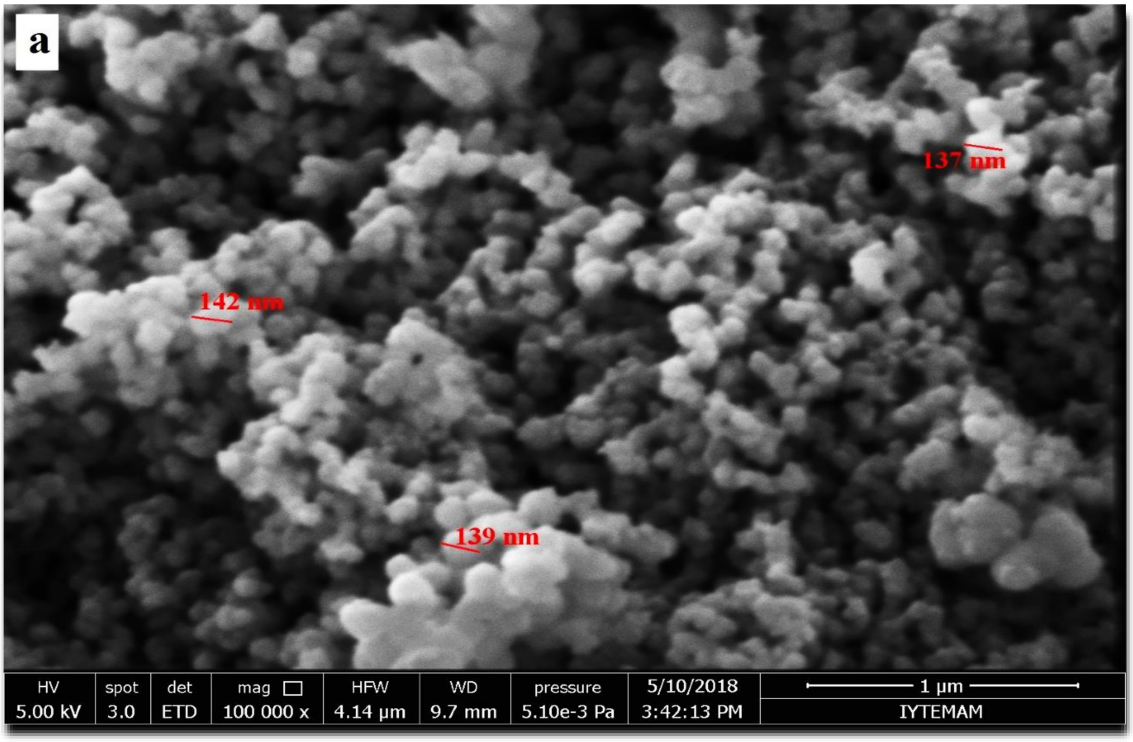

Figure 4. 2. SEM images of 0.1-0.1 mol% ZrO_2-Nd_2O_3 doped TiO_2 photocatalytic powders as precipitated and dried at 70 °C at 100 kX magnification.

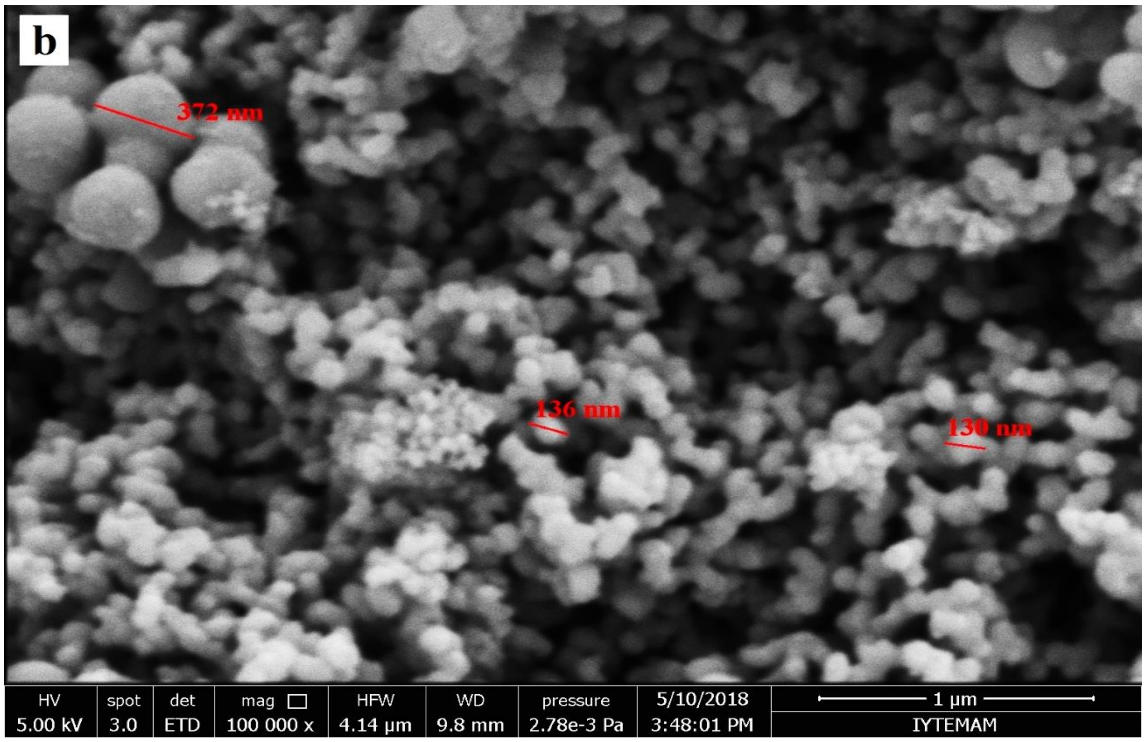

Figure 4. 3. SEM images of 0.1-0.1 mol% ZrO_2-Nd_2O_3 doped TiO_2 photocatalytic powders heat treated at 550 °C at 700 °C at 100 kX magnification.

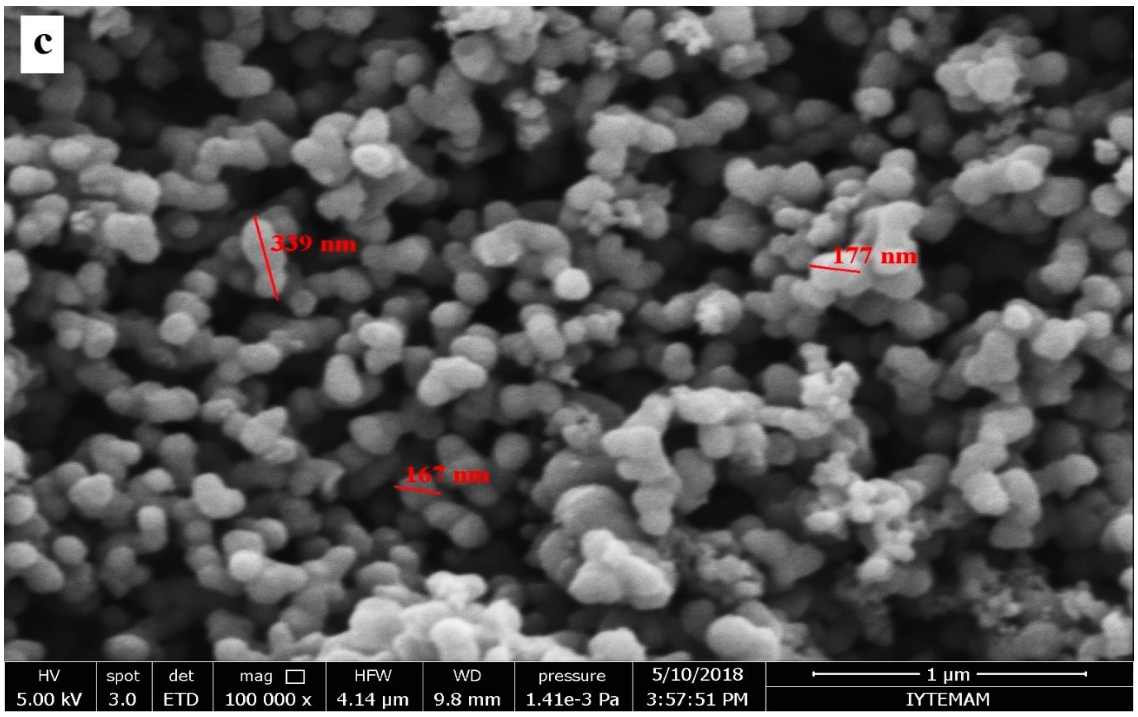

Figure 4. 4. SEM images of 0.1-0.1 mol% ZrO_2-Nd_2O_3 doped TiO_2 photocatalytic powders heat treated at 575 °C, at 100 kX magnification.

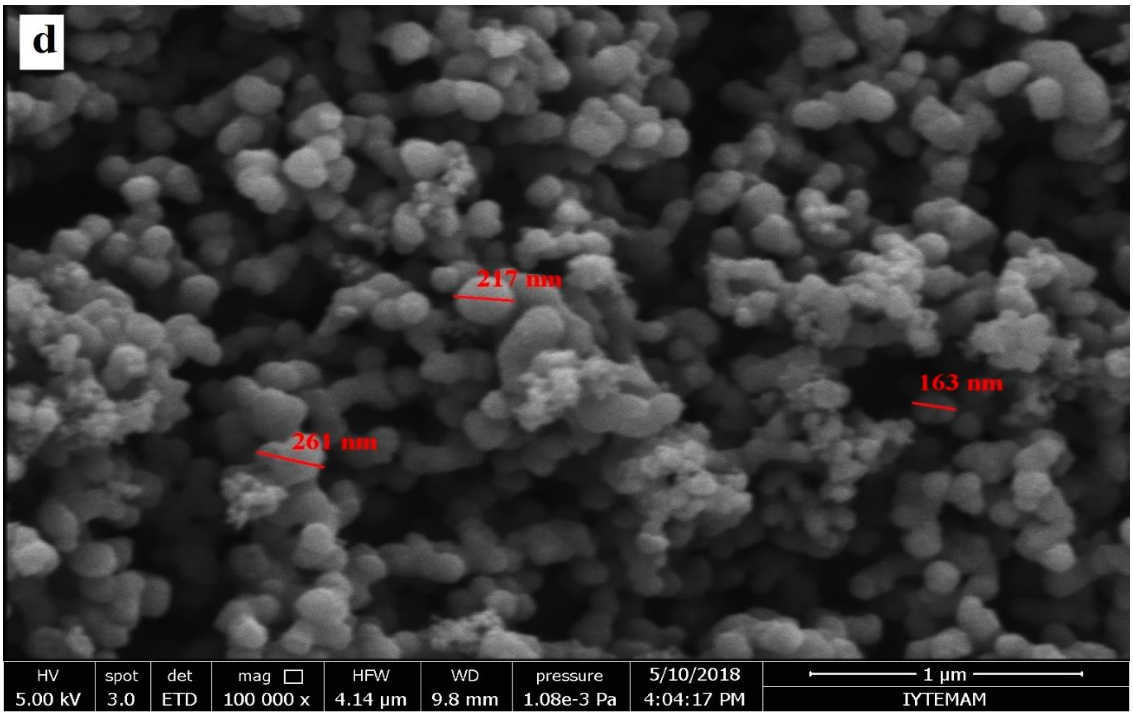

Figure 4. 5. SEM images of 0.1-0.1 mol% ZrO_2-Nd_2O_3 doped TiO_2 photocatalytic powders heat treated at 600 °C at 100 kX magnification.

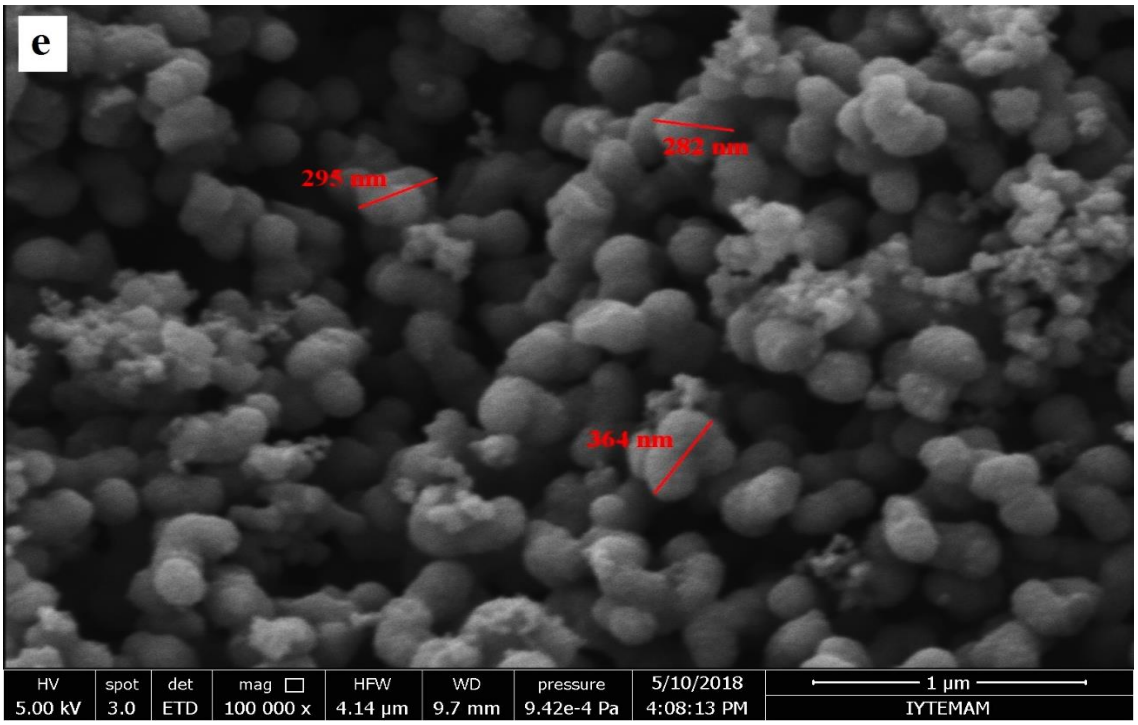

Figure 4. 6. SEM images of 0.1-0.1 mol% ZrO_2-Nd_2O_3 doped TiO_2 photocatalytic powders heat treated at 650 °C at 100 kX magnification.

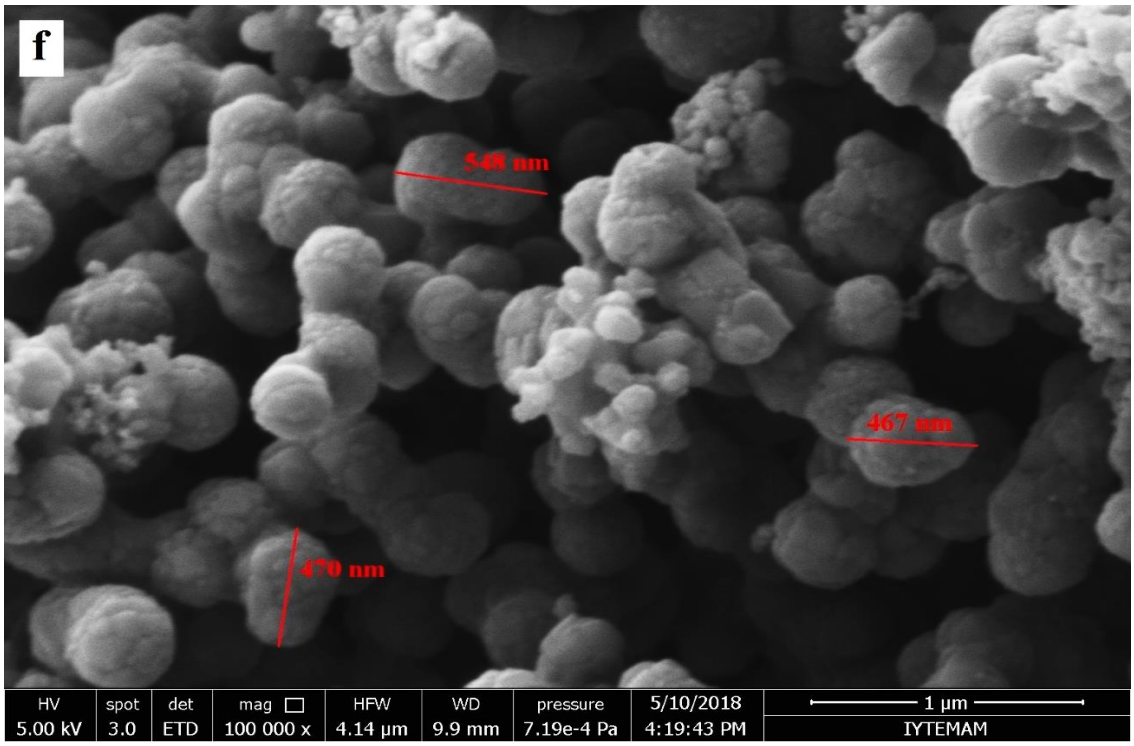

Figure 4. 7. SEM images of 0.1-0.1% ZrO_2-Nd_2O_3 doped TiO_2 photocatalytic heat treated at 700 °C at 100 kX magnification.

The average particle sizes of the 0.1-0.1 mol% ZrO_2-Nd_2O_3 doped TiO_2 photocatalytic powders determined by measuring ten particles from the SEM images at 100 kX (precipitated and dried at 70 °C, heat treated at 550 °C, 575 °C, 600 °C, 650 °C and 700 °C) are tabulated in Table 4.1. The primary particle size increases with heat treatment temperature with a likely decrease in the powder surface area. The average primary particle size of the powder heat treated at 700 °C was determined as 428 nm which is about 3.5 times bigger than the precipitated and dried powder primary particle size of about 125 nm.

Table 4. 1. Average SEM particle size of 0.1-0.1% ZrO_2-Nd_2O_3 doped TiO_2 photocatalytic powders.

0.1-0.1 mol% ZrO_2-Nd_2O_3 doped TiO_2 photocatalytic powders	**average particle size (nm)**
precipitated and dried at 70 °C	125
heat treated at 550 °C	small: 110 ; large: 338
heat treated at 575 °C	209
heat treated at 600 °C	221
heat treated at 650 °C	268
heat treated at 700 °C	428

The DLS particle size distributions of the 0.1-0.1 mol% ZrO_2-Nd_2O_3 doped TiO_2 photocatalytic powders are given in Figures 4.8 through 4.10. The Number based distributions have a single peak (131nm, 185 nm, 819 nm for dried precursor, 550°C, and 700°C respectively). These sizes are close to the SEM based sizes previously discussed. The Volume based DLS distributions are bimodal/trimodal with extra peaks located at larger sizes except the 700°C heat treated powder. These bigger particles are most likely agglomerates of primary particles/aggregates which were not completely dispersed/unbroken during sample suspension preparation for DLS analysis (5-10 minutes of ultrasonic bath treatment). The DLS particle size distrubitions of the pure TiO_2 photocatalytic powders are given in Figure 4.11 and Figure 4.12. The Number based distributions have a single peak at 160 nm and 600 nm for 550°C and 700°C. The Volume based DLS distributions have a single peak in the 700°C heat treated powder when compared with 500°C heat treated powder. The multiple peaks present were most likely due to the unbroken/undispersed agglomerates during suspension sample preparation.

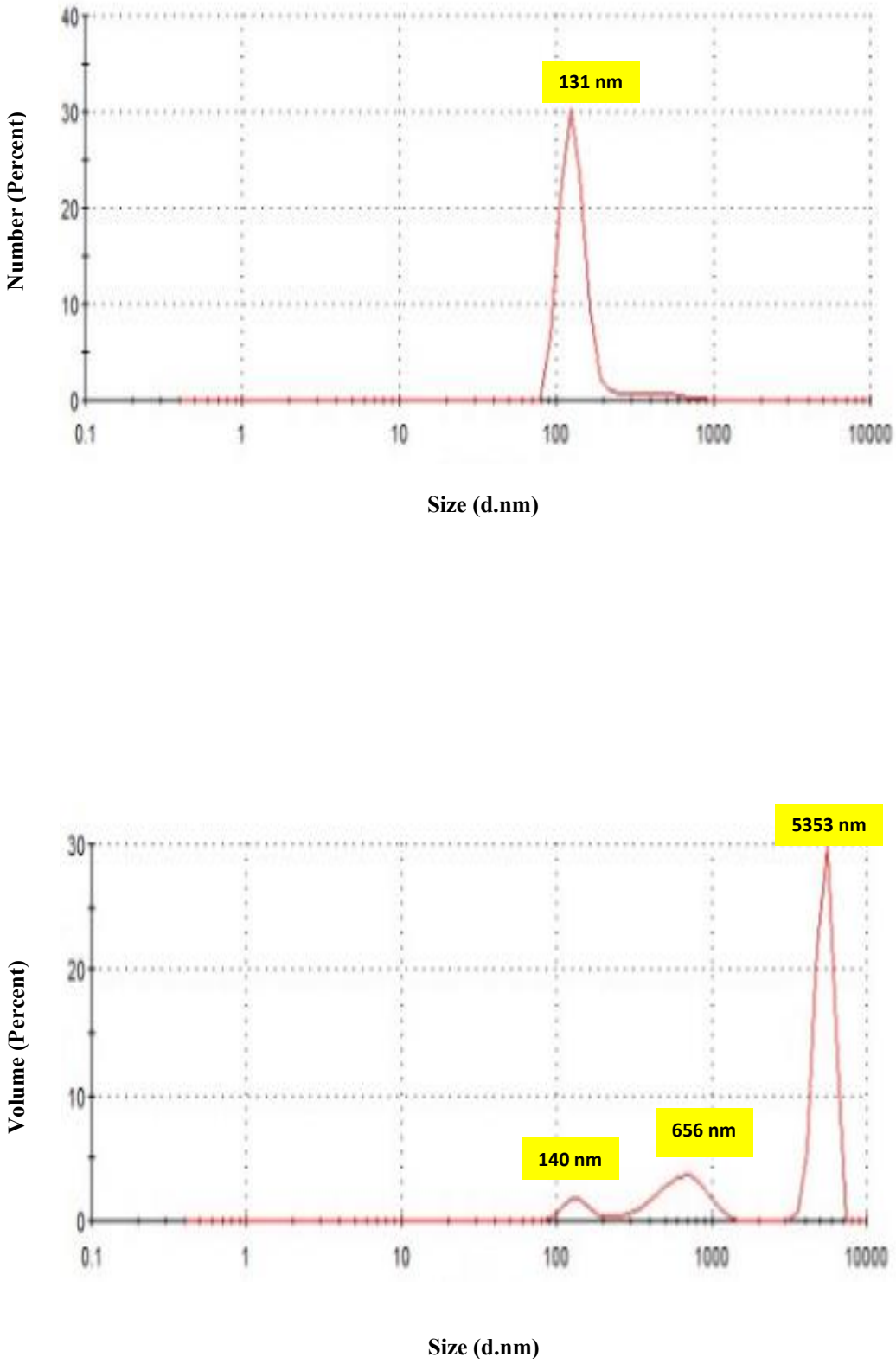

Figure 4. 8. Particle size distribution by number and volume of 0.1-0.1 mol% ZrO_2-Nd_2O_3-TiO_2 photocatalytic powder as precipitated and dried at 70 °C.

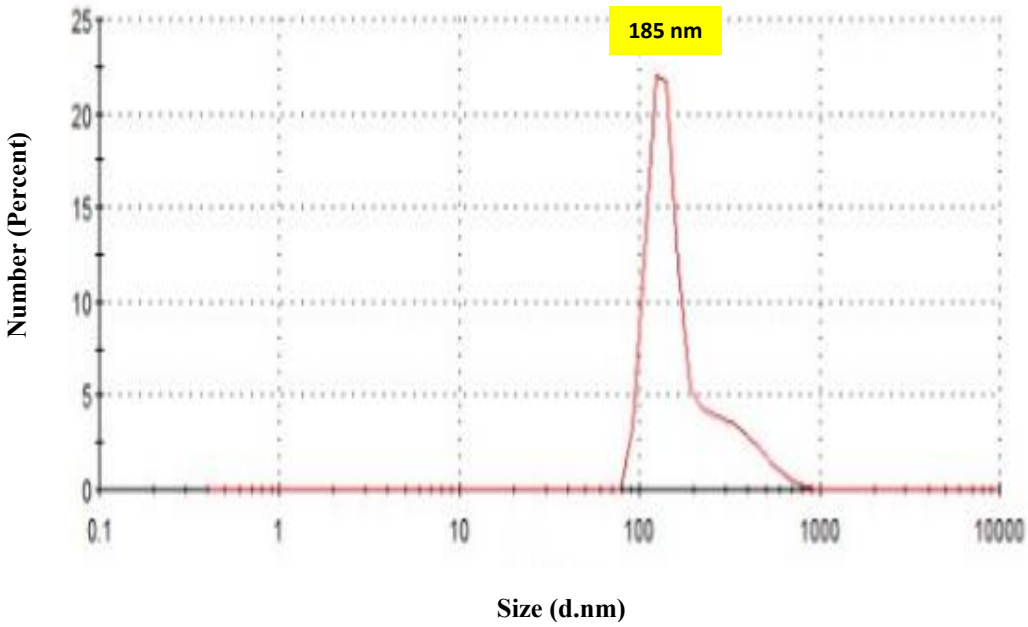

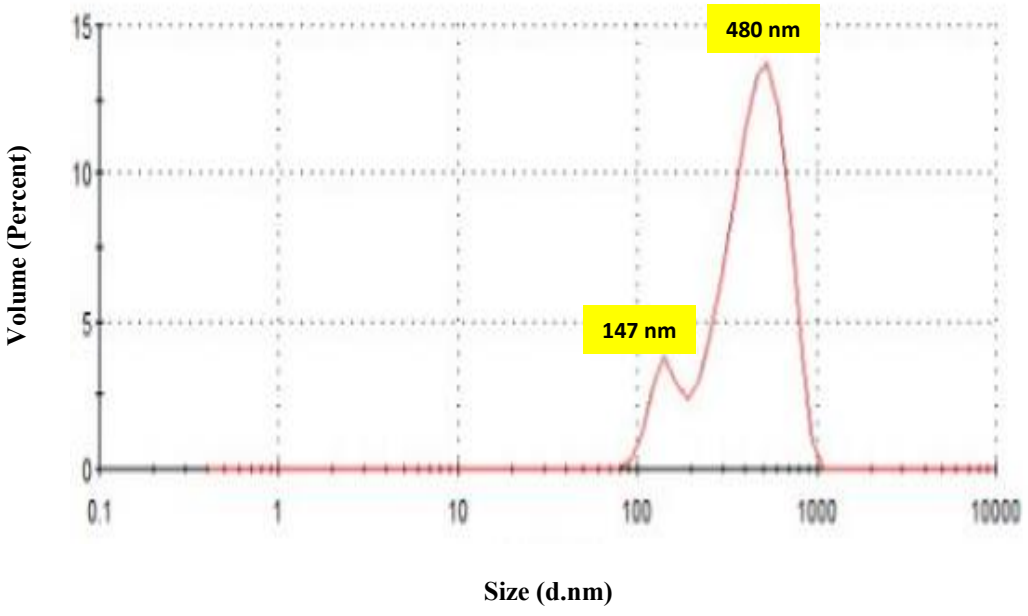

Figure 4. 9. Particle size distribution by number and volume of 0.1-0.1 mol% ZrO_2-Nd_2O_3-TiO_2 photocatalytic powder at 550 °C.

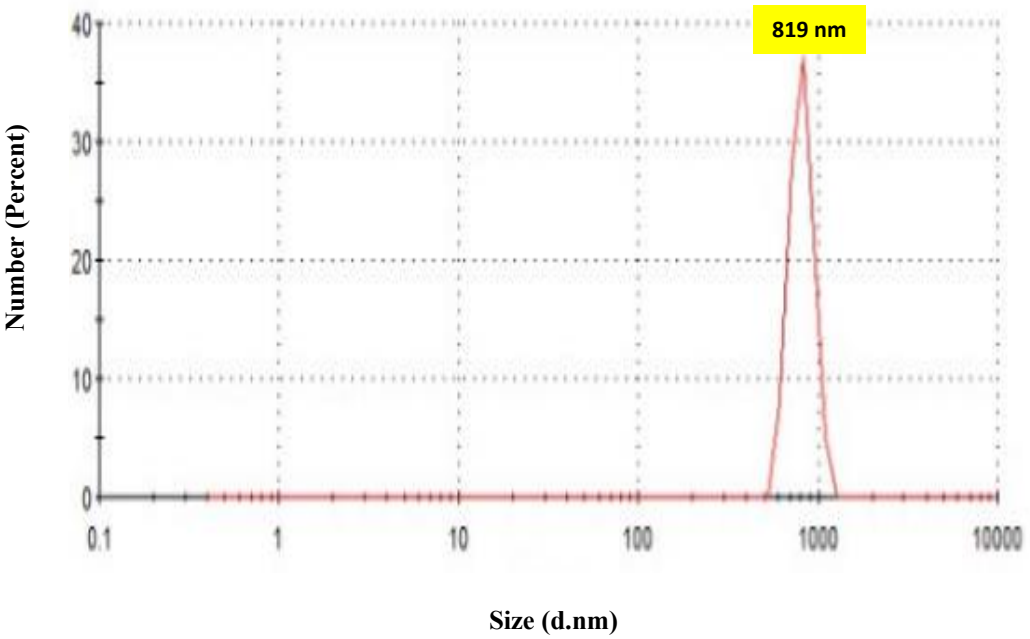

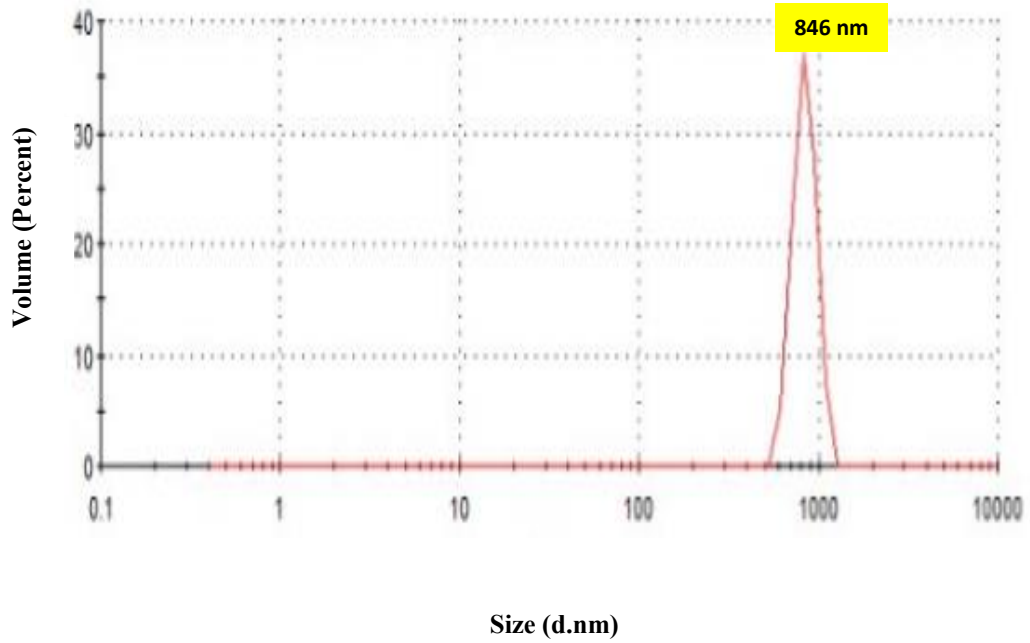

Figure 4. 10. Particle size distribution by number and volume of 0.1-0.1 mol% ZrO_2-Nd_2O_3-TiO_2 photocatalytic powder at 700 °C.

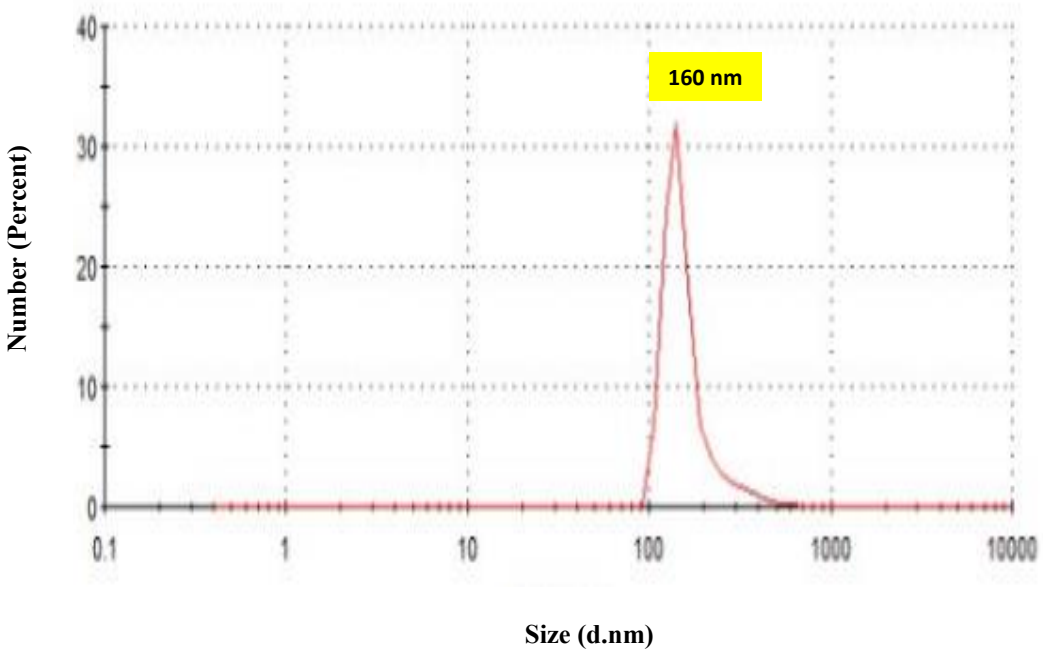

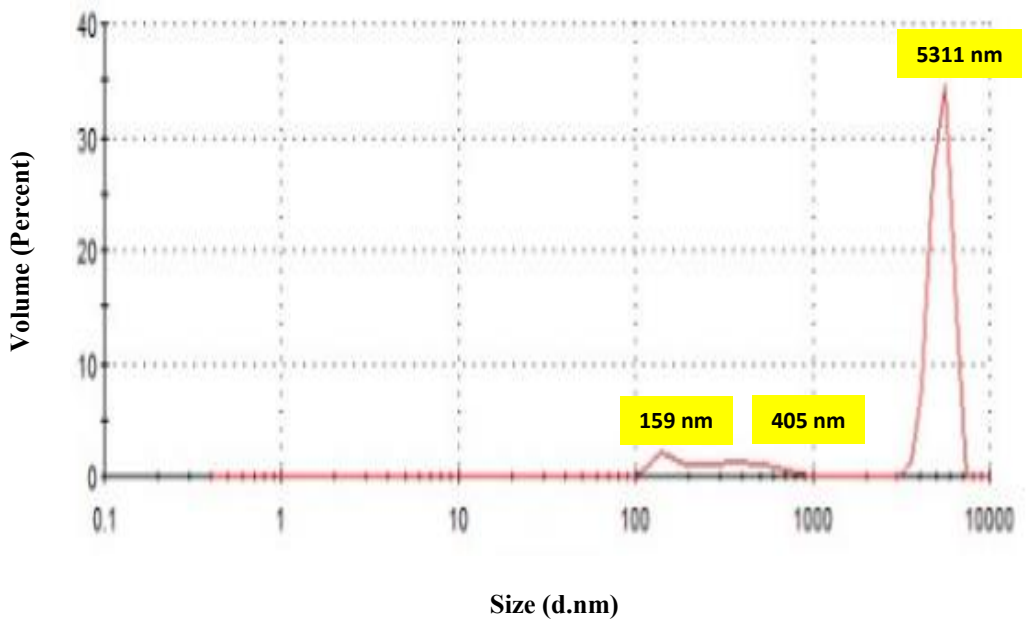

Figure 4. 11. Particle size distribution by number and volume of pure TiO_2 photocatalyic powder at 550 °C.

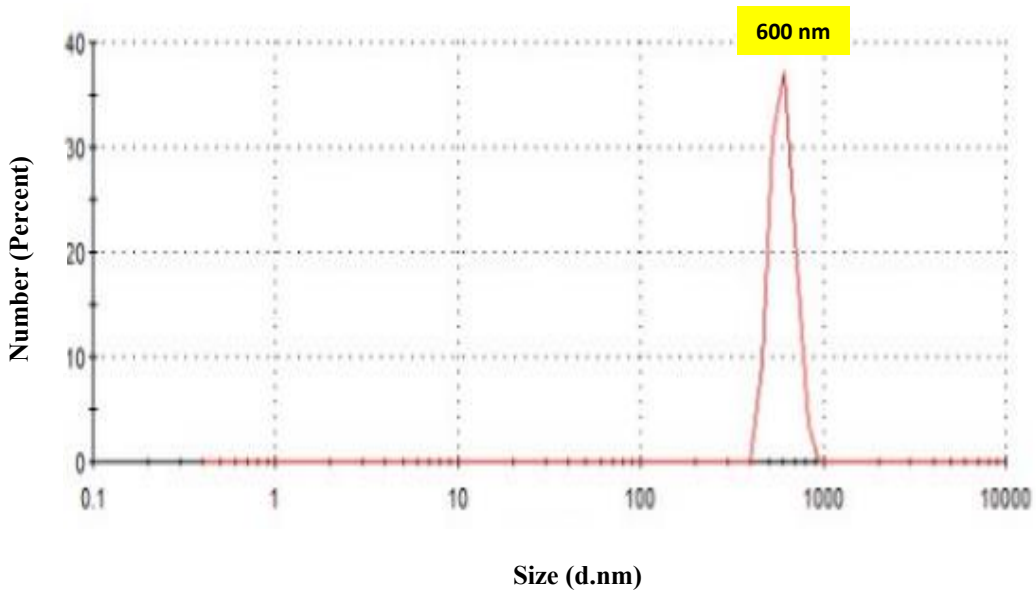

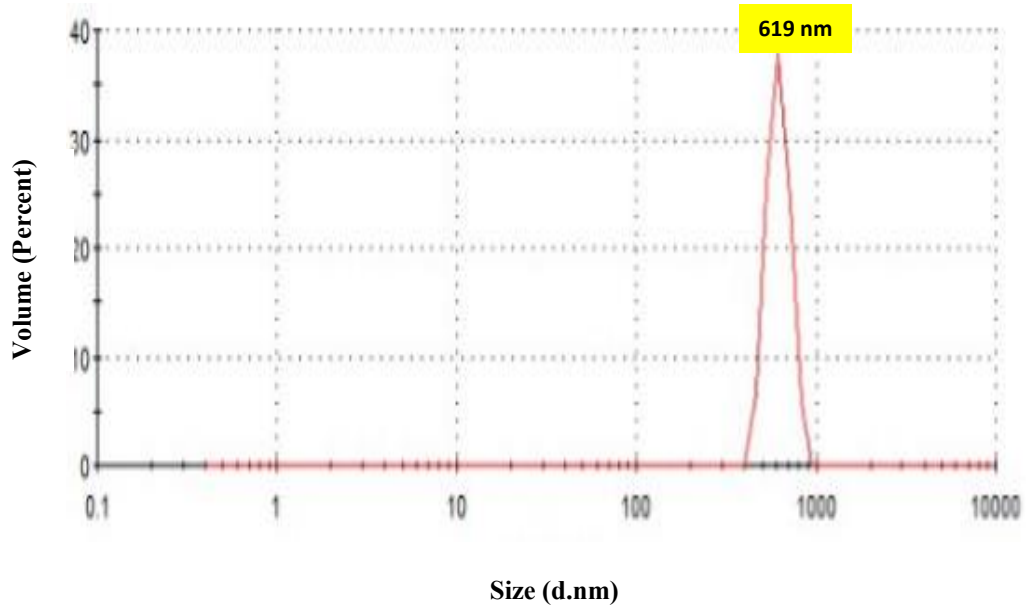

Figure 4. 12. Particle size distribution by number and volume of pure TiO_2 photocatalytic powder at 700 °C.

The XRD patterns of undoped/doped TiO_2 powders heat treated at 550 °C, 575 °C, 600 °C, 625 °C, 650 °C and 700 °C are given in Figure 4.13 and 4.18. The phase structure evolution with temperature can be determined by analyzing these patterns. The dominant phase in the 550-600C range is the anatase phase. The rutile content in the powders become higher in the 650°C-700°C range for pure TiO_2 powders. The ZrO_2 content significantly affects the phase structure evolution. The formation of the rutile phase was inhibited by ZrO_2 doping above 1 mol% up to 700°C. Rutile phase formation was prevented at 550°C with 0.1 mol% ZrO_2 and 0.1 mol% Nd_2O_3 doping. Rutile phase formation occured for the pure TiO_2 and 0.1 mol% ZrO_2 doped TiO_2 powders at 550°C. Monoclinic/tetragonal ZrO_2 phase was the dominant phase at 50% ZrO_2 loading at 650°C and 700°C whereas the structure was amorphous at 600°C at the same composition. Anatase phase was the dominant phase in 10% ZrO_2 doped TiO_2 powders up to 700°C. The phase structure and its evolution was significantly affected by the dopants even at 0.1 mol% levels used in this work.

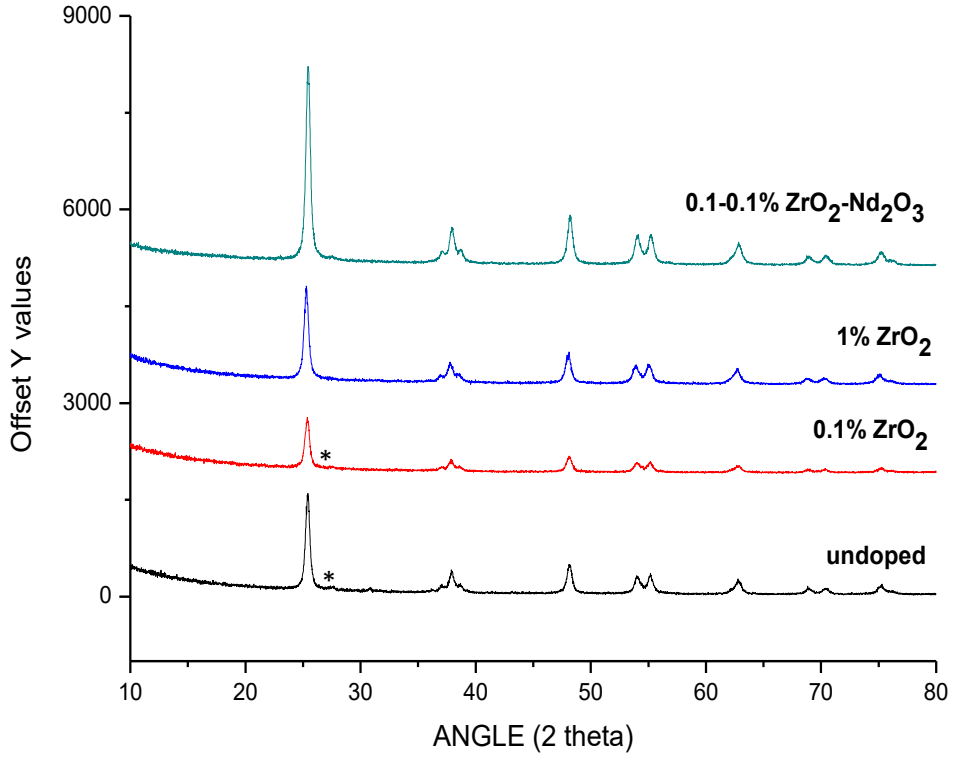

Figure 4. 13. The XRD patterns of the photocatalyst powders prepared at 550 °C. (*: rutile phase of titania)

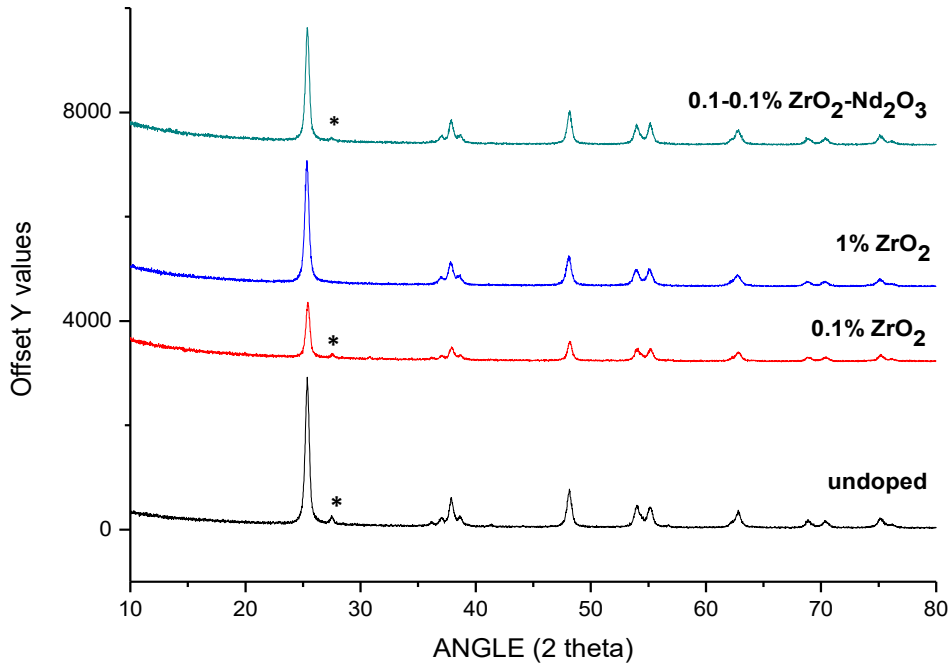

Figure 4. 14. The XRD patterns of the photocatalyst powders prepared at 575 °C. (*: rutile phase of titania)

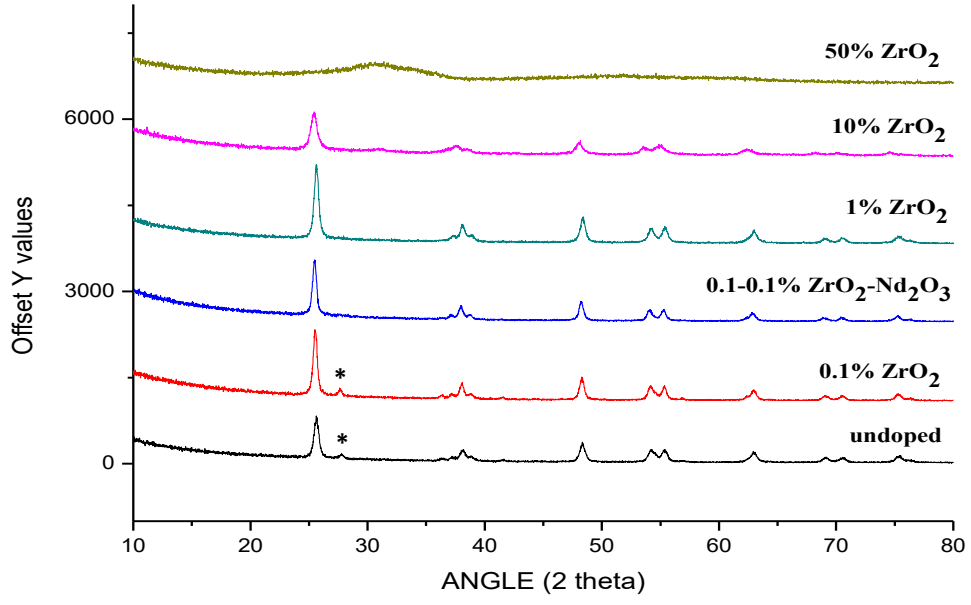

Figure 4. 15. The XRD patterns of the photocatalyst powders prepared at 600 °C. (*: rutile phase of titania)

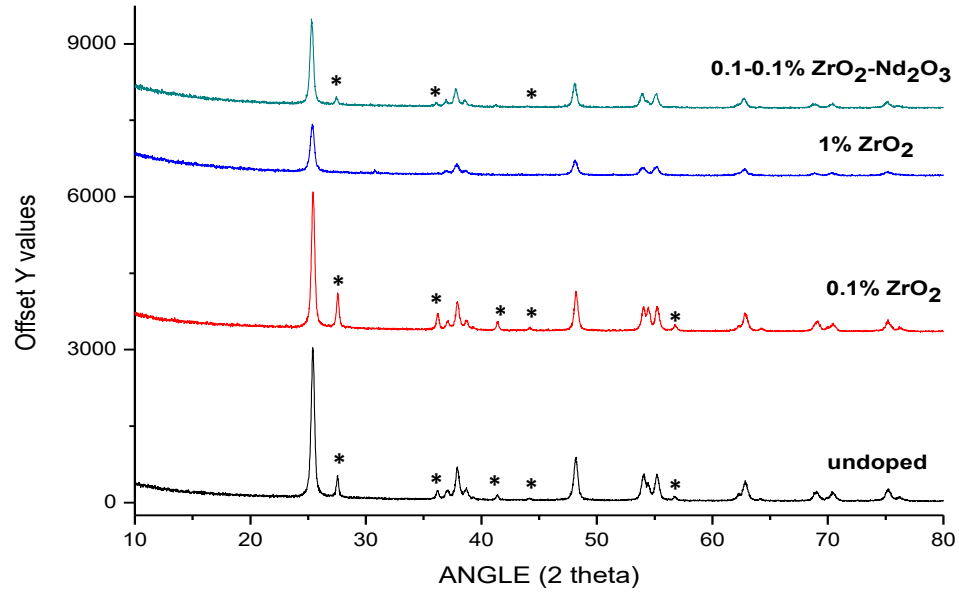

Figure 4. 16. The XRD patterns of the photocatalyst powders prepared at 625 °C. (*: rutile phase of titania)

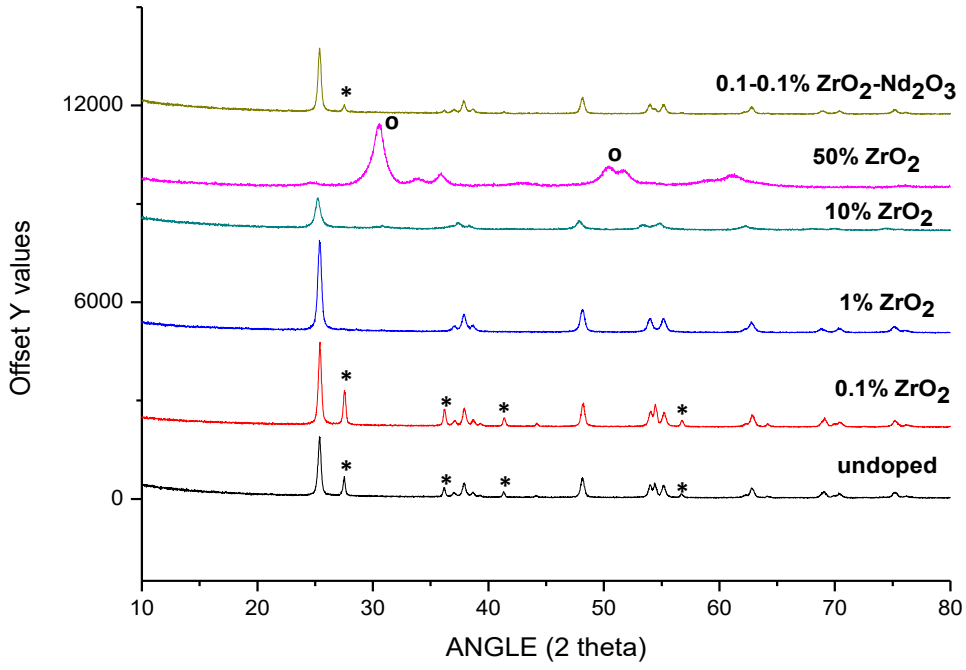

Figure 4. 17. The XRD patterns of the photocatalyst powders prepared at 650°C. (*: rutile phase of titania; o: monoclinic/tetragonal phase of zirconia)

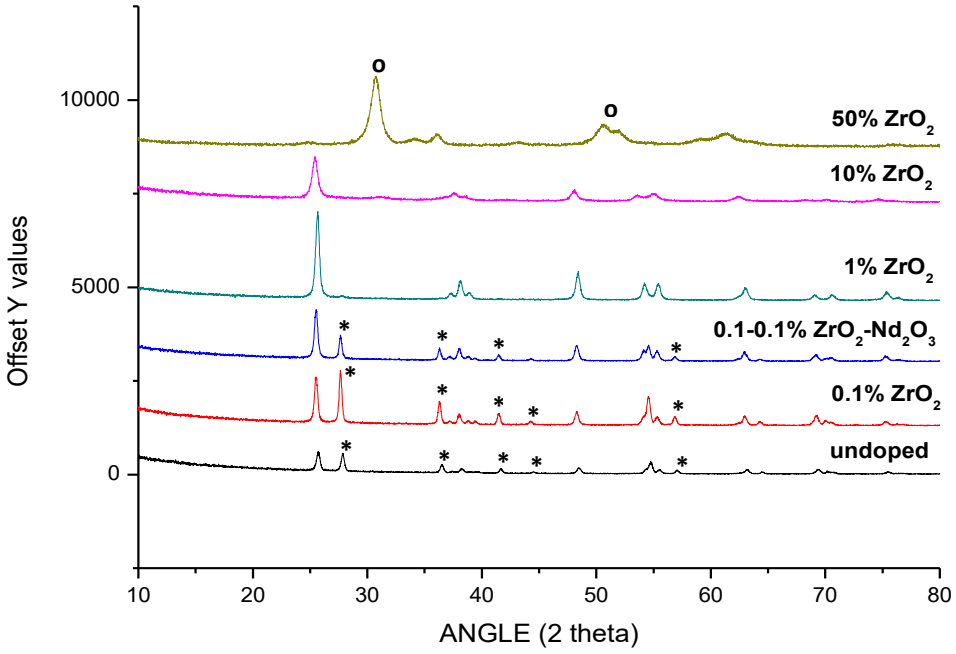

Figure 4. 18. The XRD patterns of the photocatalyst powders prepared at 700 ºC. (*: rutile phase of titania; o: monoclinic/tetragonal phase of zirconia)

4.2. Water Splitting Performance Determination

The photocatalytic water splitting and hydrogen production involves a series of important steps. These steps can be summarized as follows:

- The absorption of photons by the lattice
- The creation of the h^+/e^- pair in the VB/CB:

$$TiO_2 + h\nu \rightarrow h^+ + e^- \quad (4.1)$$

- The adsorption of the H_2O molecules on the photocatalyst surface
- The oxidation reactions between the h+ and the adsorbed water molecules and the formation of H^+ ions and •OH radicals:

$$H_2O + h^+ \rightarrow H^+ + \cdot OH \quad (4.2)$$

- The reduction of cupric ions by photogenerated electrons:

$$Cu(II) + e^-_{CB} \rightarrow Cu(I) + e^-_{CB} \rightarrow Cu(0) \quad (4.3)$$

- The oxidation of the sacrificial organic species by photogenerated positive holes:

$$S_{ads} + h^{+}_{VB} \rightarrow S_{ox} + H^{+} \quad (4.4)$$

- The reduction reactions for H_2 formation:

$$H^{+} \xrightarrow{e^{-}} \cdot H \rightarrow \cdot H + \cdot H \rightarrow H_2 \quad (4.5)$$

- The oxidation reactions for O_2 formation:

$$\cdot OH + \cdot OH \rightarrow H_2\ O_2 \xrightarrow{h^{+}} O_2^{-} + 2H^{+} \xrightarrow{h^{+}} O_2 \quad (4.6)$$

- The recombination reactions:

$$TiO_2(excited) + h^{+} + e^{-} \rightarrow TiO_2 \quad (4.7)$$

The sequence of these events is further schematically shown in Figure 4.19.

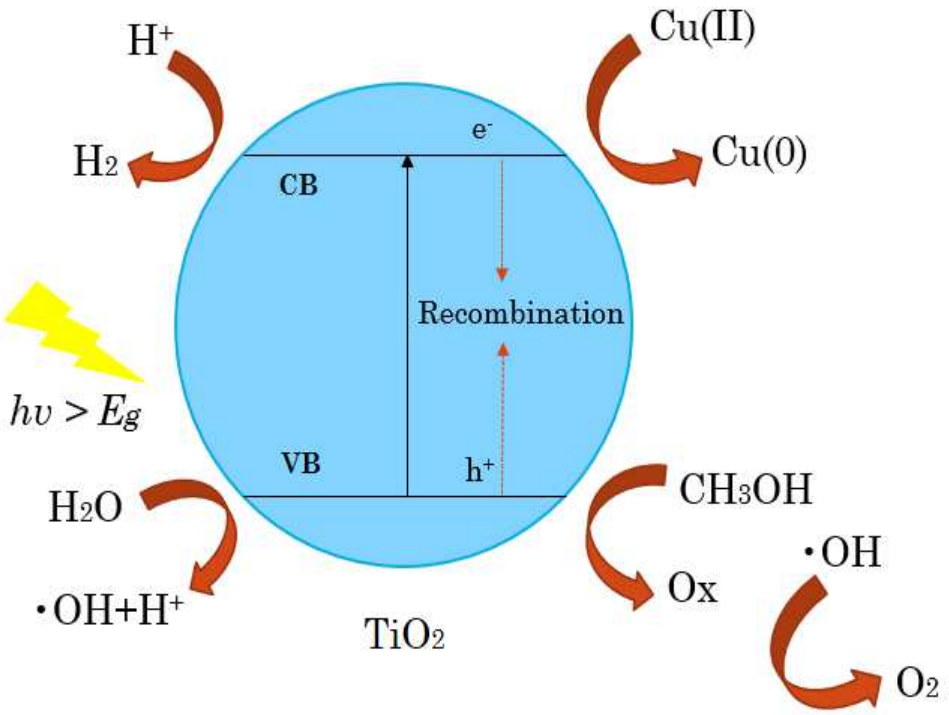

Figure 4. 19. Basic mechanism of overall water splitting on a semiconductor particle with copper photodeposition.

The rate of these proposed reaction steps heavily depend on the photocatalyst phase and electronic structure (band-gap) along with surface area and properties. These material properties can be varied by the composition and heat treatment temperature of the photocatalyst. This was accomplished by the use of ZrO_2 and Nd_2O_3 dopants in the TiO_2 matrix followed by heat treatment in the 550-700°C in this work.

The photocatalytic activities of the prepared ZrO_2 and ZrO_2-Nd_2O_3 doped TiO_2 powders heat treated at various temperatures were determined by Gas Chromatography. Hydrogen yields were determined during 3 hours in these experiments. The determined hydrogen yields are plotted as a function of time in three hours in Figures 4.20-4.25. The hydrogen yields obtained in three hours are further plotted as a function of dopant composition in Figures 4.26 and 4.27.

The hydrogen yield of 10 mol% ZrO_2-TiO_2 and 50 mol% ZrO_2-TiO_2 photocatalytic powders were significantly lower than pure TiO_2 powders as seen in Figures 4.22, 4.25 and 4.27. The higher band-gap of the zirconia rich phases and their related poor UV-Vis light absorption properties is most likely responsible for this behaviour. The results of this work indicated that doping above 10% ZrO_2 decreases the rate of photon absorption/h+/e- generation significantly. The same plots have shown that doping at 1 mol% level generates a favorable phase/electronic structure for water splitting reaction sequence except 550ºC as can be clearly seen in Figure 4.26.

The Nd_2O_3 doped powders had significantly higher activities as shown in Figure 4.28 at almost all heat treatment temperatures. This maybe attributed to the enhanced light absorption in the visible region. 0.1-0.1 mol% ZrO_2-Nd_2O_3-TiO_2 photocatalytic powder at 550°C had the highest photocatalytic activity among all which was about 5000 μmol/g.

The copper photodeposition increases the hydrogen yield of 0.1 mol% ZrO_2-Nd_2O_3-TiO_2 photocatalyst powder approximately 5 times as seen in Figure 4.20. The hydrogen yield of pure TiO_2 was about 3000-3500 μmol/g which was higher than ZrO_2 and ZrO_2- Nd_2O_3 doped photocatalytic powders heat treated at 700°C as shown in Figure 4.25. This may be due to a favorable phase composition (Anatase-rutile combination) for the undoped powder.

The 0.1-0.1 mol% ZrO_2-Nd_2O_3 doped photocatalyst had the highest hydrogen yield at 550°C in this work which was about twice that of 0.1 mol% ZrO_2 doped photocatalyst as can seen from Figure 4.20. This may be attributed to the better light absorption in the visible/infrared region due to the presence of Nd (Yurtsever and Çiftçioğlu 2017). The hydrogen yield increases linearly with time. ZrO_2 doping at this

very low level increases hydrogen yield almost two times when compared to undoped titania which may due to the changes related with the phase structure (rutile phase formation suppression/crystallite size reduction). ZrO_2 doping at a 1 mol% level did not effect the hydrogen yield at this temperature.

The hydrogen yield of 1 mol% ZrO_2 doped photocatalyst is the highest at 575°C which was about twice that of undoped TiO_2. This may be due to the retardation of TiO_2 phase transformations which was reported in earlier thesis work conducted in our laboratories (Yaltık, K., MSc Thesis, 2017). The differences in the surface areas of the powders may also be responsible for the differences in photocatalytic activies of the powders at this temperature due to rapid densification of the undoped powders (Duvarcı and Çiftçioğlu 2012). Nd_2O_3 doping also increases the hydrogen yield at this temperature. The ZrO_2 doping at this low level may cause the formation of a defective surface/bulk structure along with the stabilization of the anatase phase. The ionic radii of Ti^{4+} and Zr^{4+} is reported to be about 68 and 72 pm respectively which may greatly favor substitutional cation replacement during the precipitation/further phase evolution during haet treatment. The reported bandgaps of the oxide phases present in the photocatalytic powders prepared in this work are as follows:Anatase TiO_2-Rutile TiO_2 in the 3-3.2 eV and rutile has a slightly lower value, ZrO_2:3.4-5.7 eV depending on the phase structure and powder processing/properties, and Nd_2O_3:4.0 eV. The bandgaps of photocatalyst powders are commonly known to be highly sensitive to even very low levels of both metallic and nonmetallic dopants.

The low levels of ZrO_2 at 0.1 and 1 mol% may modify the electronic structure/lower the bandgap/create both surface/bulk defects/oxygen vacancies which may cause a faster and more efficient visible/UV light absorption which may significantly facilitate the h+/e- couple generation. The hydrogen yields of the ZrO_2 doped powders at the lowest two levels (0.1 and 1 mol%) at lower heat treatment temperatures (600-650°C) which can be seen in Figures 22 and 24 were determined to be significantly higher than pure TiO_2. This may be due to the generation sub electronic states in the structure enhancing light absorption and the increased surface area caused by the retarded densification/phase transformation with doping.

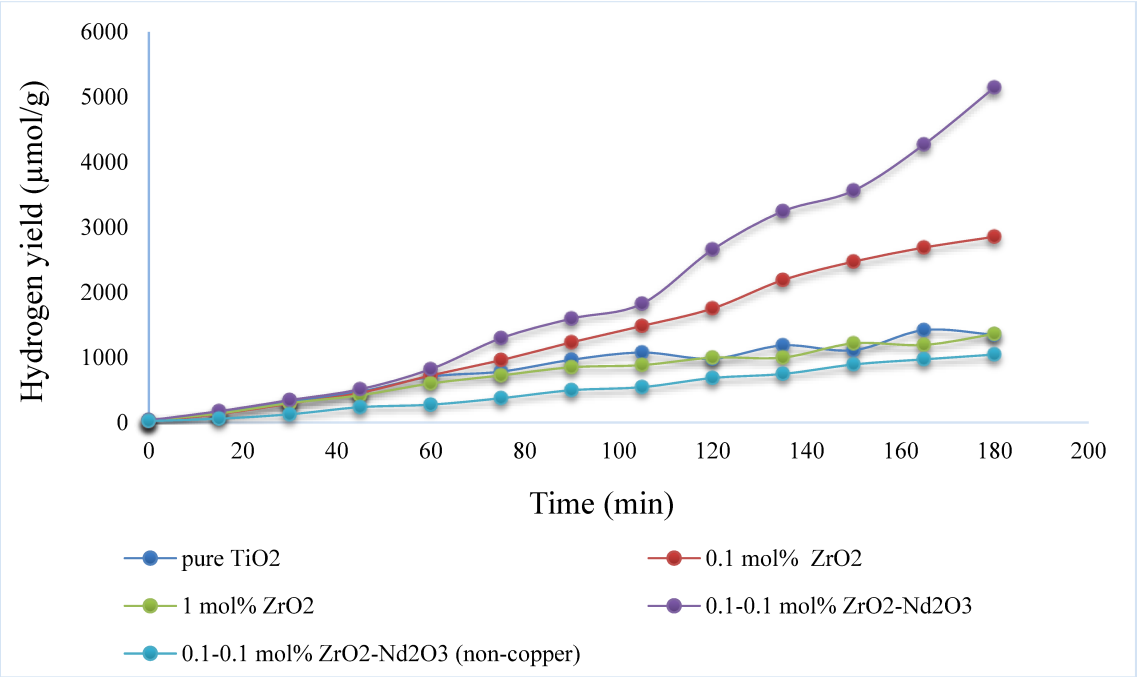

Figure 4. 20. Hydrogen yield (µmol/g) vs time (min) graphs for pure TiO_2, 0.1 mol% ZrO_2-TiO_2, 0.1-0.1 mol% ZrO_2-Nd_2O_3-TiO_2, 1 mol% ZrO_2-TiO_2 and 0.1-0.1 mol% ZrO_2-Nd_2O_3-TiO_2 (non-copper) at 550 °C heat treatment.

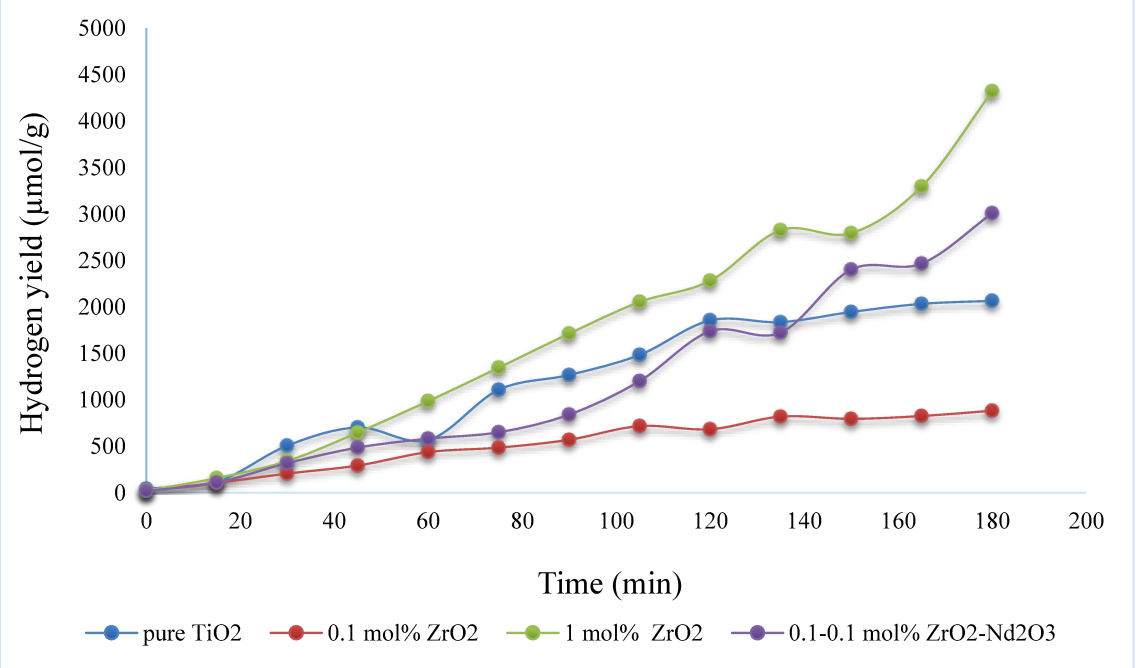

Figure 4. 21. Hydrogen yield (µmol/g) vs time (min) graphs for pure TiO_2, 0.1 mol% ZrO_2-TiO_2, 0.1-0.1 mol% ZrO_2-Nd_2O_3-TiO_2 and 1 mol% ZrO_2-TiO_2 at 575 °C heat treatment.

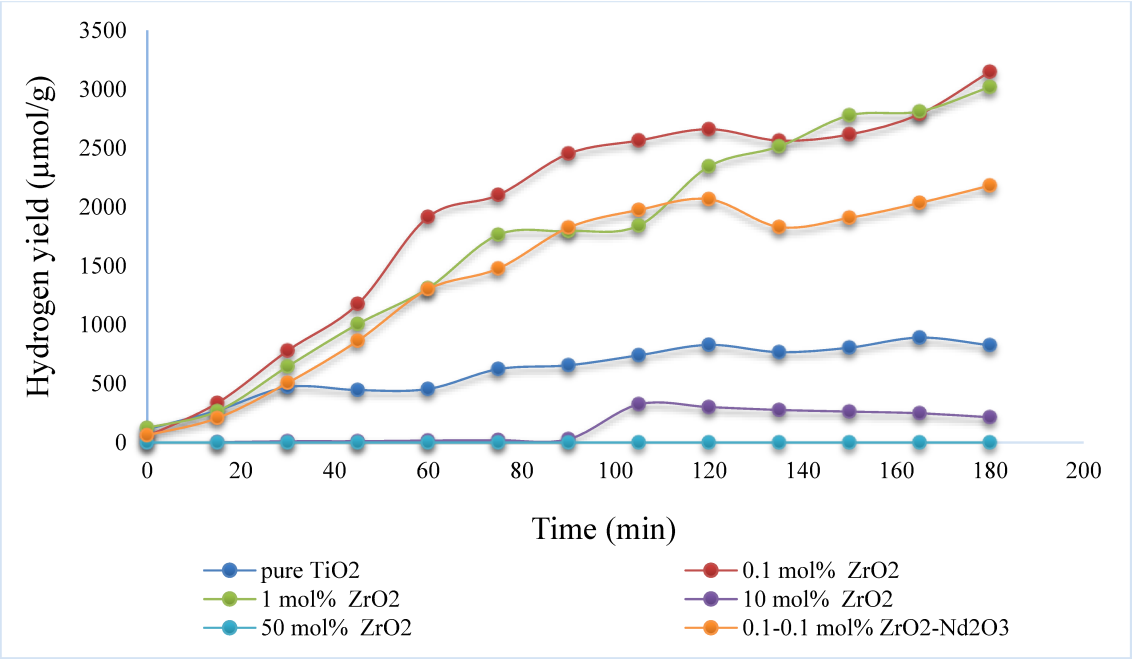

Figure 4. 22. Hydrogen yield (µmol/g) vs time (min) graphs for pure TiO_2, 0.1 mol% ZrO_2-TiO_2, 0.1-0.1 mol% ZrO_2-Nd_2O_3-TiO_2, 1 mol% ZrO_2-TiO_2, 10 mol% ZrO_2-TiO_2 and 50 mol% ZrO_2-TiO_2 at 600 °C heat treatment.

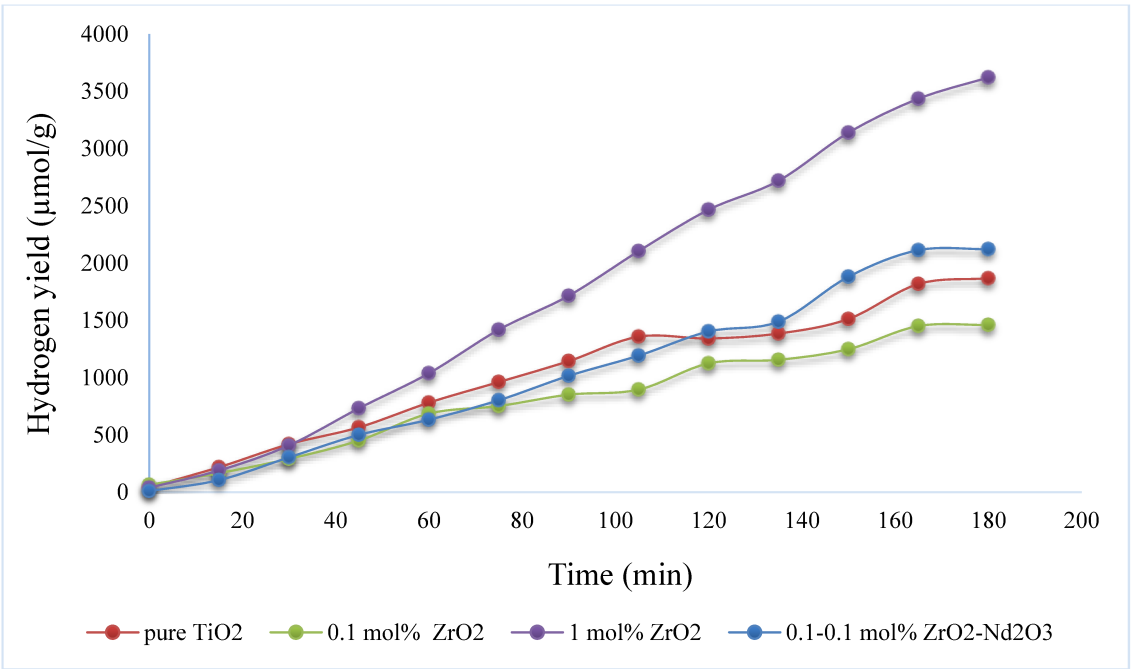

Figure 4. 23. Hydrogen yield (µmol/g) vs time (min) graphs for pure TiO_2, 0.1 mol% ZrO_2-TiO_2, 0.1-0.1 mol% ZrO_2-Nd_2O_3-TiO_2 and 1 mol% ZrO_2-TiO_2 at 625 °C heat treatment.

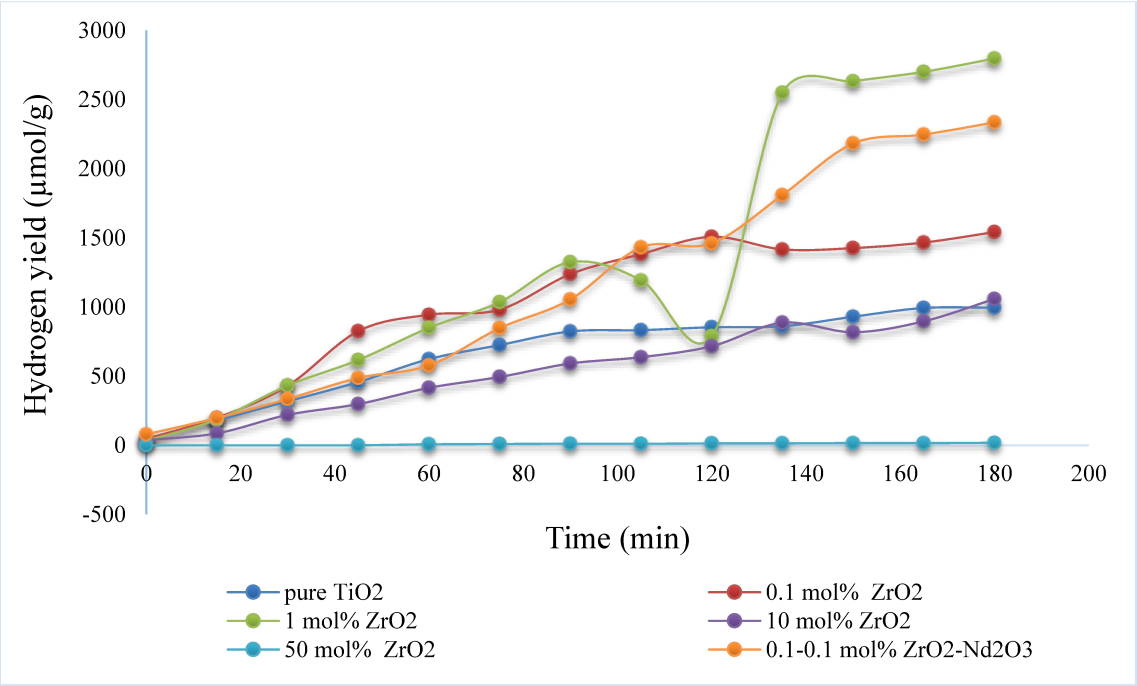

Figure 4. 24. Hydrogen yield (µmol/g) vs time (min) graphs for pure TiO_2, 0.1 mol% ZrO_2-TiO_2, 0.1-0.1 mol% ZrO_2-Nd_2O_3-TiO_2, 1 mol% ZrO_2-TiO_2, 10 mol% ZrO_2-TiO_2 and 50 mol% ZrO_2-TiO_2 at 650 °C heat treatment.

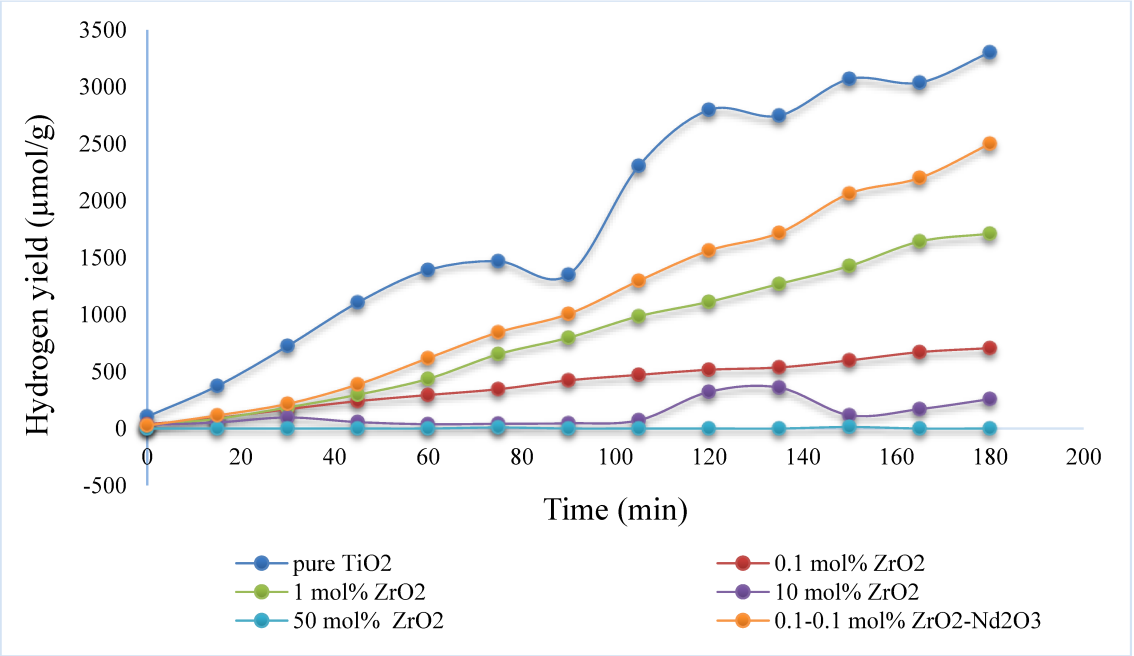

Figure 4. 25. Hydrogen yield (µmol/g) vs time (min) graphs for pure TiO_2, 0.1 mol% ZrO_2-TiO_2, 0.1-0.1 mol% ZrO_2-Nd_2O_3-TiO_2, 1 mol% ZrO_2-TiO_2, 10 mol% ZrO_2-TiO_2 and 50 mol% ZrO_2-TiO_2 at 700 °C heat treatment.

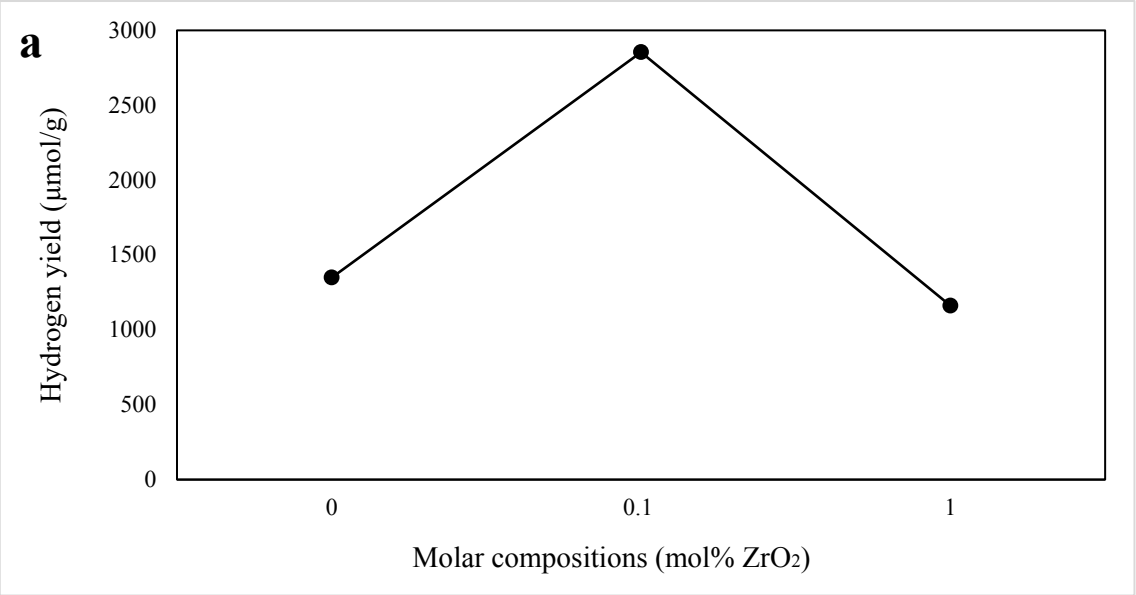

Figure 4. 26. Hydrogen yield (µmol/g) vs molar compositions (mol% ZrO_2) graphs for pure TiO_2, 0.1 mol% ZrO_2-TiO_2, 1 mol% ZrO_2-TiO_2 at (a) 550°C, (b) 575°C, and (c) 625°C heat treatment. **(Cont. on next page)**

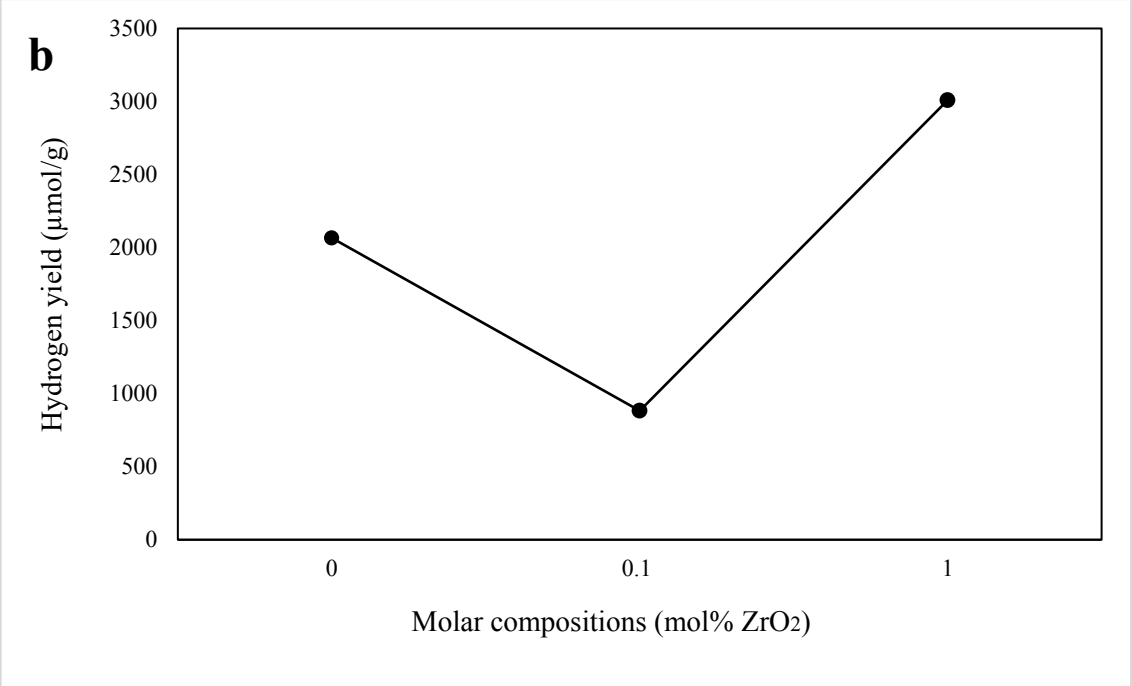

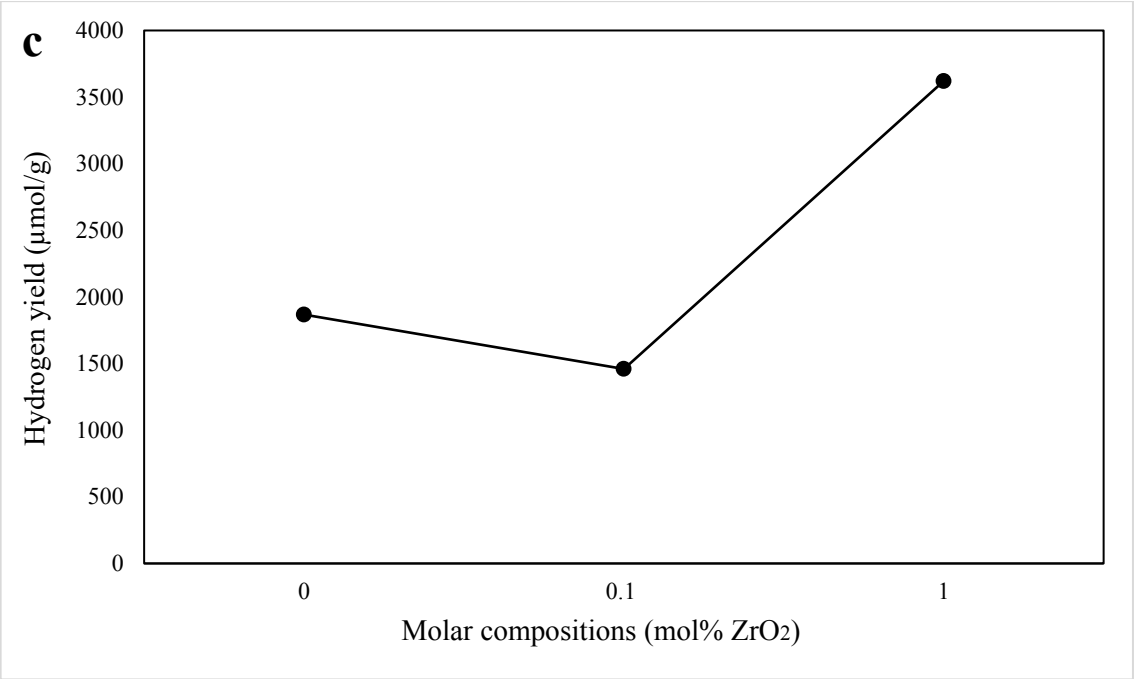

Figure 4.26 (Cont.)

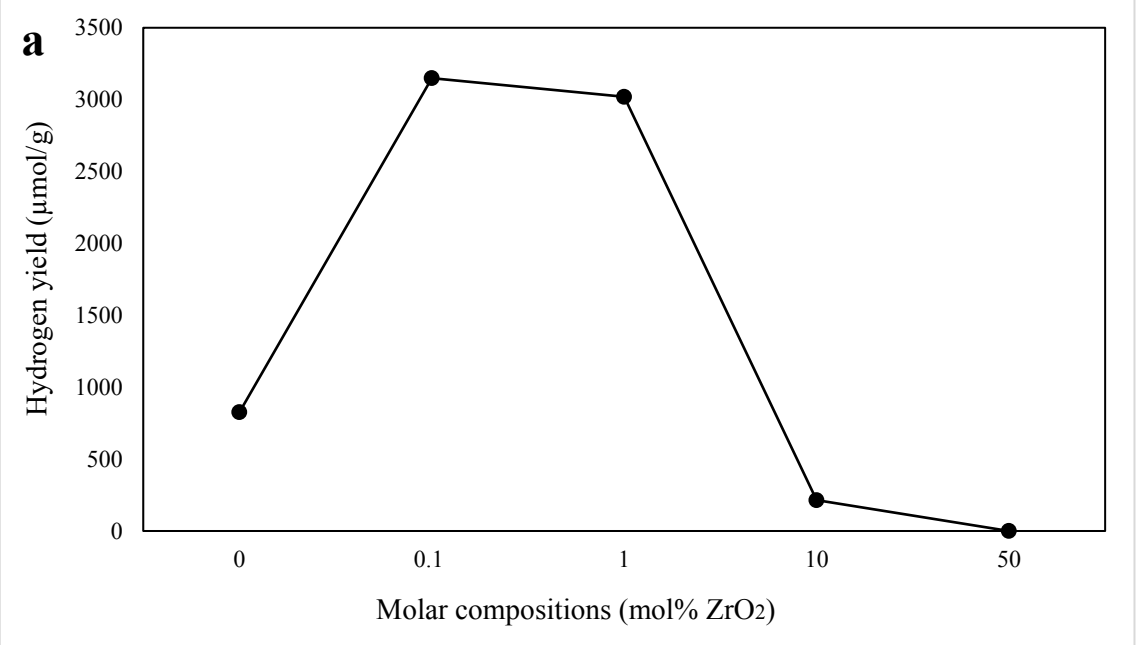

Figure 4. 27. Hydrogen yield (µmol/g) vs molar compositions (mol% ZrO_2) for pure TiO_2, 0.1 mol% ZrO_2-TiO_2, 1 mol% ZrO_2-TiO_2, 10 mol% ZrO_2-TiO_2 and 50 mol% ZrO_2-TiO_2 at (a) 600°C, (b) 650°C, and (c) 700 °C heat treatment. **(Cont. on next page)**

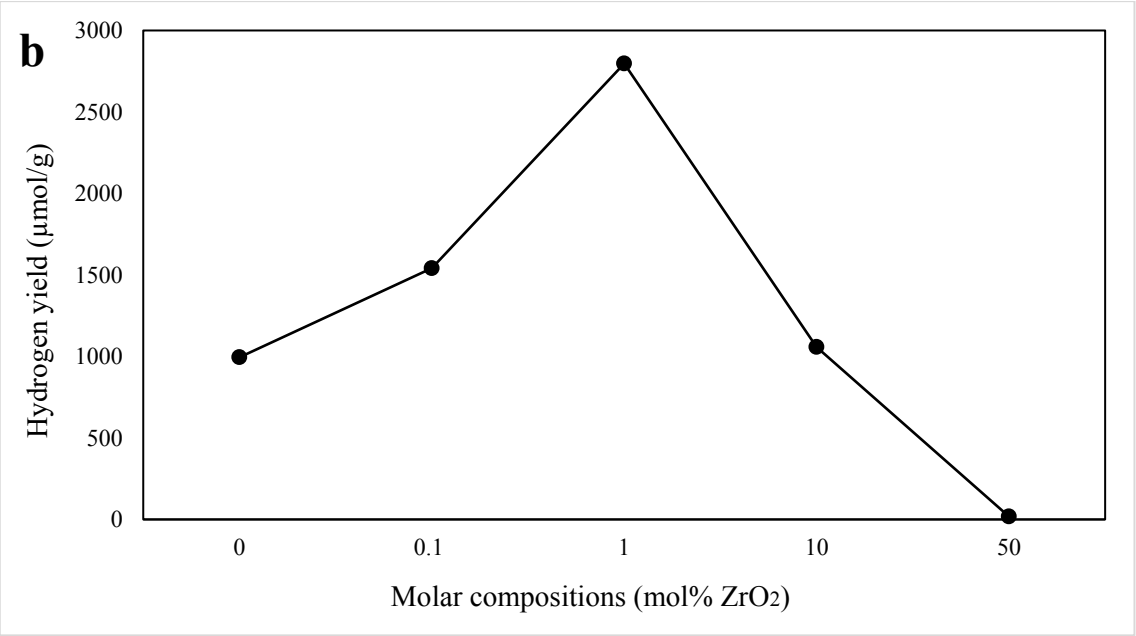

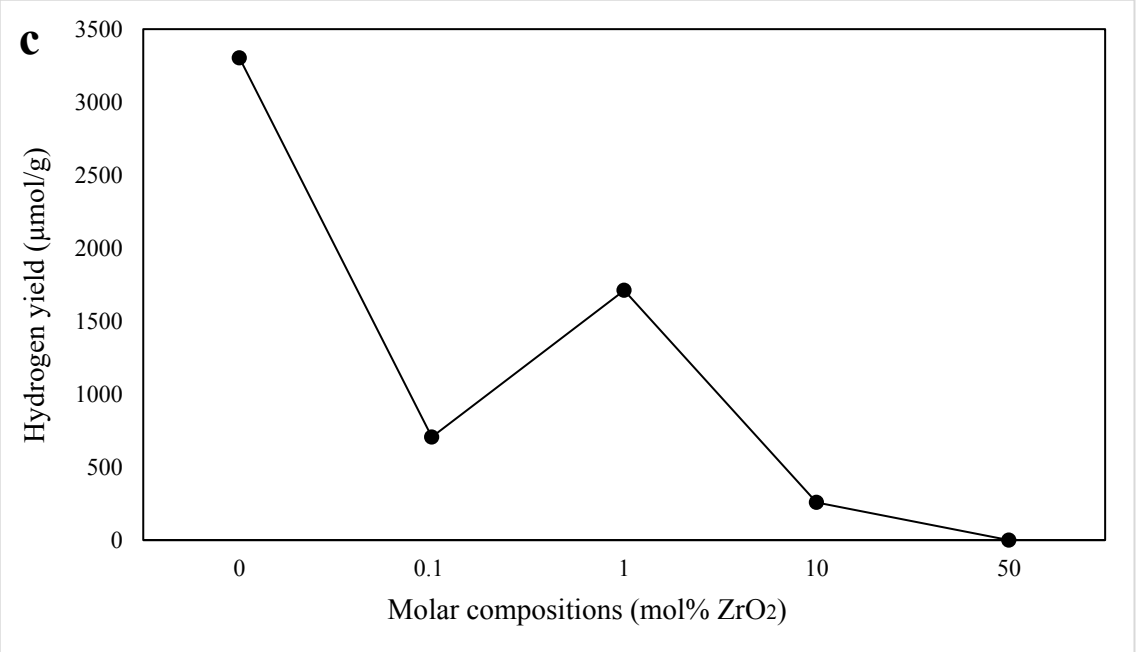

Figure 4.27 (Cont.)

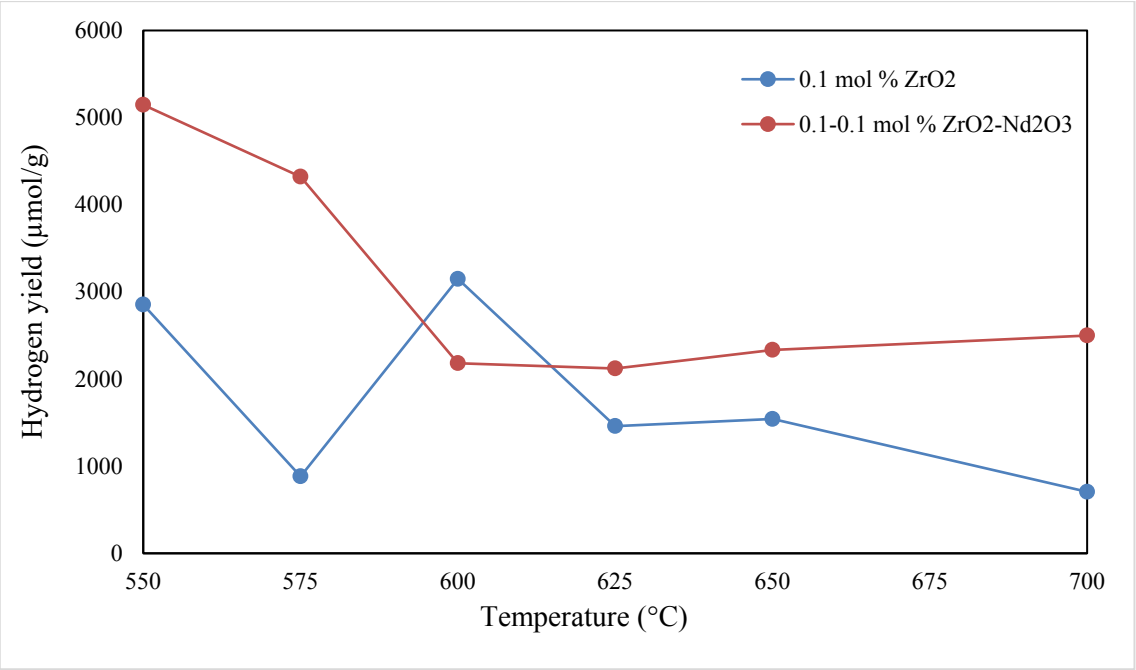

Figure 4. 28. Hydrogen yield (µmol/g) vs temperature (°C) graphs for 0.1 mol% ZrO_2-TiO_2 and 0.1-0.1 mol% ZrO_2-Nd_2O_3-TiO_2 in the 550-700 °C heat treatment range.

CHAPTER 5

CONCLUSIONS AND RECOMMENDATIONS

The increase of average temperatures around the world (both land and water) and it's atmosphere have occured since 1976. The temperature increase of the Earth was mostly due to natural reasons in the past. The increase nowadays is mostly caused by the accumulation of greenhouse gases in the atmosphere produced by human activities. The use of nonrenewable fossil fuels for satisfying the increasing energy needs of humanity accounts for the majority of these gases. The use of cleaner fuels like hydrogen can be an important solution to this problem. The use of sunlight through photocatalysis and artificial photosynthesis in the production of hydrogen and other hydrocarbons through completing carbon cycle presents a promising solution. Intensive research activities are currently conducted globally on artificial photosynthesis.

TiO_2 is a very commonly used and investigated semiconductor in photocatalytic processes due to its superior chemical stability. Intensive research on the effects of various dopants on the properties of the most stable titania phases anatase and rutile in enhancing its visible light absorption and photocatalytic abilities is currently being conducted. This global effort is directed on the development of a better understanding on the effects of these dopants on the phase/electronic structure and the most important steps of the photocatalytic water splitting process.

The effect of ZrO_2 doping on the phase/electronic structure of TiO_2 in the 0-50 mol% doping range was investigated in this study. The powders were coprecipitated from an alcoholic media by using alkoxide precursors. The sizes of the equiaxed primary precipitated particles were about 140 nm. The particle size increased up to about 500 nm through the thermal treatment of these powders in the 550-700°C range which was determined by SEM images and DLS particle size distributions. The TiO_2 phase transformation from the anatase to the rutile phase was significantly suppressed by the dopants. Monoclinic/Tetragonal ZrO_2 was the dominant phase at 50 mol% dopant content at 700°C.

The water splitting abilities of these powders under UV-Vis light was investigated through the determination of their hydrogen yields during 3 hour photocatalytic reactions by using a GC system. The highest hydrogen yields were obtained for the 0.1-0.1 mol%

ZrO_2-Nd_2O_3 photocatalyts heat treated at 550°C as about 5000 μmol/hr gcat. The zirconia dopant extents above 10 mol% decreased the water splitting abilities of the TiO_2 based photocatalysts most likely due to poor absorption of light/increased band-gap energies.

The water splitting abilities/properties of TiO_2- ZrO_2-Nd_2O_3 photocatalysts in the 0-5 mol% ZrO_2-Nd_2O_3 doping range may generate useful information in future work. The nanodesign of micron sized oxide composite structures may also be investigated towards the preparation of photocatalysts with enhanced water splitting abilities/easy removal from the catalysis medium.

REFERENCES

Al-Rasheed, Radwan A. 2005. "Water Treatment by Heterogeneous Photocatalysis an Overview." Presented at 4th SWCC Acquired Experience Symposium, Jeddah, 2005.

Brotosudarmo, Tatas H. P., Monika N. U. Prihastyanti, Alastair T. Gardiner, Anne-Marie Carey, and Richard J. Cogdell. 2014. "The Light Reactions of Photosynthesis as a Paradigm for Solar Fuel Production." *Energy Procedia* 47:283-289.

Byrne, Ciara, Gokulakrishnan Subramanian, and Suresh C. Pillai. 2017. "Recent advances in photocatalysis for environmental applications." *Journal of Environmental Chemical Engineering* 1-60.

Castellote, Marta , and Nicklas Bengtsson. 2011. "Principles of TiO_2 Photocatalysis." In *Application of Titanium Dioxide Photocatalysis to Construction Materials*, edited by Yoshihiko Ohama and Dionys Van Gemert, 5-10. New York: Springer.

Clarizia, Laura, Giuseppe Vitiello, Giuseppina Luciani, Ilaria Di Somma, Roberto Andreozzi, and Raffaele Marotta. 2016. "In situ photodeposited nanoCu on TiO_2 as a catalyst for hydrogen production under UV/visible radiation." *Applied Catalysis A: General* 518:142-149.

Diebold, Ulrike. 2003. "The surface science of titanium dioxide." *Surface Science Reports* 48:53-229.

Duvarcı, Ö. Çağlar and Muhsin Çiftçioğlu. 2012. "Preparation and characterization of nanocrystalline titania powders by sonochemical synthesis." *Powder Technology* 228: 231-240.

El-Khouly, Mohamed E., Eithar El-Mohsnawy, and Shunichi Fukuzumi. 2017. "Solar energy conversion: From natural to artificial photosynthesis." *Journal of Photochemistry and Photobiology C: Photochemistry Reviews* 31:36-83.

Freije, Afnan Mahmood, Tahani Hussain, and Eman Ali Salman. 2018. "Global warming awareness among the University of Bahrain science students." *Journal of the Association of Arab Universities for Basic and Applied Sciences* 22 (1):9-16.

Fujishima, Akira, and Kenichi Honda. 1972. "Electrochemical Photolysis of Water at a Semiconductor Electrode." *Nature* 238:37-38.

Fujishima, Akira, Tata N. Rao, and Donald A. Tryk. 2000. "Titanium dioxide photocatalysis." *Journal of Photochemistry and Photobiology C: Photochemistry Reviews* 1:1–21.

Hammarstrom, Leif, and Sharon Hammes-Schiffer. 2009. "Artificial Photosynthesis and Solar Fuels." *Accounts of Chemical Research* 42 (12):1859-1860.

Hassan, M. Shamshi, Touseef Amna, O. Bong Yang, Hyun-Chel Kim, and Myung-Seob Khil. 2012. "TiO_2 nanofibers doped with rare earth elements and their photocatalytic activity." *Ceramics International* 38 (7):5925-5930.

Hoffmann, Michael R., Scot T. Martin, Wonyong Choi, and Detlef W. Bahnemannt. 1995. "Environmental Applications of Semiconductor Photocatalysis." *Chem. Rev.* 95:69-96.

House, Ralph L., Neyde Yukie Murakami Iha, Rodolfo L. Coppo, Leila Alibabaei, Benjamin D. Sherman, Peng Kang, M. Kyle Brennaman, Paul G. Hoertz, and Thomas J. Meyer. 2015. "Artificial photosynthesis: Where are we now? Where can we go?" *Journal of Photochemistry and Photobiology C: Photochemistry Reviews* 25:32-45.

Ibhadon, Alex, and Paul Fitzpatrick. 2013. "Heterogeneous Photocatalysis: Recent Advances and Applications." *Catalysts* 3 (1):189-218.

Ismail, Adel A., and Detlef W. Bahnemann. 2014. "Photochemical splitting of water for hydrogen production by photocatalysis: A review." *Solar Energy Materials and Solar Cells* 128:85-101.

Kabir, Ehsanul, Pawan Kumar, Sandeep Kumar, Adedeji A. Adelodun, and Ki-Hyun Kim. 2018. "Solar energy: Potential and future prospects." *Renewable and Sustainable Energy Reviews* 82:894-900.

Khan, Mohammad Mansoob, Syed Farooq Adil, and Abdullah Al-Mayouf. 2015. "Metal oxides as photocatalysts." *Journal of Saudi Chemical Society* 19 (5):462-464.

Kokporka, Lawan, Surakerk Onsuratoom, Tarawipa Puangpetch, and Sumaeth Chavadej. 2013. "Sol–gel-synthesized mesoporous-assembled TiO_2–ZrO_2 mixed oxide nanocrystals and their photocatalytic sensitized H_2 production activity under visible light irradiation." *Materials Science in Semiconductor Processing* 16 (3):667-678.

Lan, Yucheng, Yalin Lu, and Zhifeng Ren. 2013. "Mini review on photocatalysis of titanium dioxide nanoparticles and their solar applications." *Nano Energy* 2 (5):1031-1045.

Lindsey, Rebecca and LuAnn Dahlman. 2018. "Global temperature vs. year from 1901 to 2000." *Climate.gov*, August 1, 2018. https://www.ncdc.noaa.gov/.

Michael J. Farabee. 2006. "Photosynthesis." *Estrella Mountain Community College*. Last modified June 24, 2001. https://www2.estrellamountain.edu/.

Mohanta, Pulok Ranjan , Jigar Patel, Jayesh Bhuva, and Misal Gandhi. 2015. "A Review on Solar Photovoltaics and Roof Top Application of It." *International Journal of Advance Research in Engineering, Science & Technology(IJAREST)* 2 (4):2394-2444.

Molinari, R., A. Caruso, and L. Palmisano. 2010. “Photocatalytic Processes in Membrane Reactors.” In *Comprehensive Membrane Science and Engineering*, edited by Enrico Drioli and Lidietta Giorno,165-193. United Kingdom: Elsevier.

Nguyen, Van-Huy, and Jeffrey C. S. Wu. 2018. “Recent developments in the design of photoreactors for solar energy conversion from water splitting and CO_2 reduction.” *Applied Catalysis A: General* 550:122-141.

Ni, Meng, Michael K. H. Leung, Dennis Y. C. Leung, and K. Sumathy. 2007. “A review and recent developments in photocatalytic water-splitting using TiO_2 for hydrogen production.” *Renewable and Sustainable Energy Reviews* 11 (3):401-425.

Onsuratoom, Surakerk, Sumaeth Chavadej, and Thammanoon Sreethawong. 2011. “Hydrogen production from water splitting under UV light irradiation over Ag-loaded mesoporous-assembled TiO_2–ZrO_2 mixed oxide nanocrystal photocatalysts.” *International Journal of Hydrogen Energy* 36 (9):5246-5261.

Onsuratoom, Surakerk, Tarawipa Puangpetch, and Sumaeth Chavadej. 2011. “Comparative investigation of hydrogen production over Ag-, Ni-, and Cu-loaded mesoporous-assembled TiO_2–ZrO_2 mixed oxide nanocrystal photocatalysts.” *Chemical Engineering Journal* 173 (2):667-675.

Pliekhov, Oleksii, Olena Pliekhova, Yusuf Osman Donar, Ali Sınağ, Nataša Novak Tušar, and Urška Lavrenčič Štangar. 2017. “Enhanced photocatalytic activity of carbon and zirconium modified TiO_2.” *Catalysis Today* 284:215-220.

R. Reddy, Vangala, Dong Won Hwang, and Jae Sung Lee. 2003. “Photocatalytic Water Splitting over ZrO2 Prepared by Precipitation Method.” *Korean J. Chem. Eng.* 20 (6):1026-1029.

Shon, Hokyong, Yousef Okour, Ibrahim El Saliby, Jun Park, Dong-Lyun Cho, Jong Beom Kim, Hee Ju Park, and Jong-Ho Kim. 2009. “Preparation and Characterisation of Titanium Dioxide Produced from Ti-salt Flocculated Sludge in Water Treatment.” *J. Korean Ind. Eng. Chem* 20, (3):241-250.

Sigmund, Wolfgang, Hassan El-Shall, Dinesh O. Shah, and Brij M. Moudgil. 2009. *Particulate Systems in Nano- and Biotechnologies*. Boca Raton, FL: CRC Press.

U.S Energy Information Administration. 2018. “Annual Energy Outlook 2018 with projections to 2050.” Accessed February 24, 2018. https://www.eia.gov/outlooks/aeo/pdf/AEO2018.pdf.

Woodley, S. M., and C. R. A. Catlow. 2009. “Structure prediction of titania phases: Implementation of Darwinian versus Lamarckian concepts in an Evolutionary Algorithm.” *Computational Materials Science* 45 (1):84-95.

Yaltrık, Kaan. 2017. “Preparation and application of subnano ceramic filtration membranes for organic species removal from aqueous streams.” Master of Science Thesis, Chemical Engineering, İzmir Institute of Technology.

Yin, Z. F., L. Wu, H. G. Yang, and Y. H. Su. 2013. "Recent progress in biomedical applications of titanium dioxide." *Phys Chem Chem Phys* 15 (14):4844-58.

Yurtsever, Hüsnü Arda. 2015. "Preparation and characterization of titania based powders and suspensions for photocatalytic applications." Doctoral Thesis, Chemical Engineering, İzmir Institute of Technology.

Yurtsever, H. Arda and Muhsin Çiftçioğlu 2017, "The effect of rare earth element doping on the microstructural evolution of sol-gel titania powders.*" Journal of Alloys and Compounds* 695: 1336-1353.

Zhang, Jianqi, Li Li, Jingjing Zhang, Xinyue Zhang, and Wenzhi Zhang. 2017. "Controllable design of natural gully-like TiO_2–ZrO_2 composites and their photocatalytic degradation and hydrogen production by water splitting." *New Journal of Chemistry* 41 (17):9113-9122.

Zhu, Zhen, Cheng-Tse Kao, Bing-Hong Tang, Wei-Chen Chang, and Ren-Jang Wu. 2016. "Efficient hydrogen production by photocatalytic water-splitting using Pt-doped TiO_2 hollow spheres under visible light." *Ceramics International* 42 (6):6749-6754.